Optimization of Gap Bridging Performance in Laser Butt Welding Using Beam Shaping Technology

Exploring the Application of Beam Shaping in Mass-Production

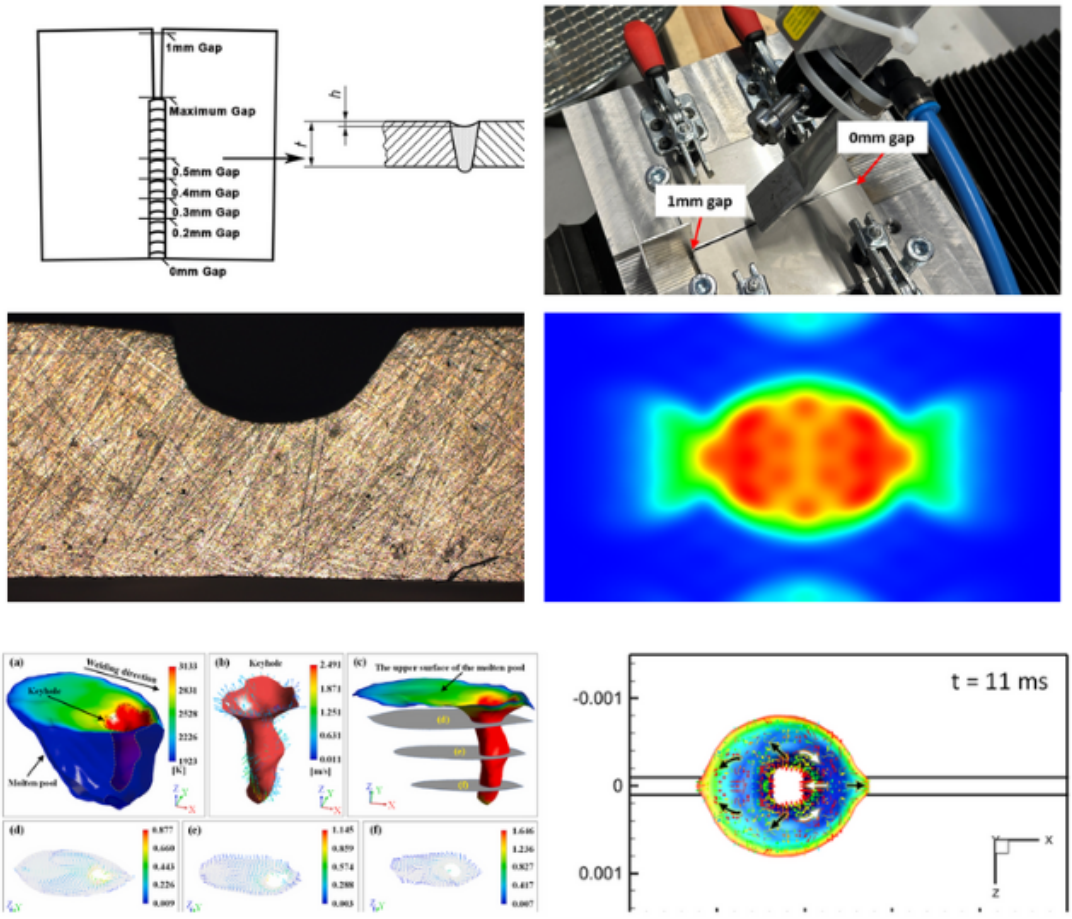

VT Master Project

Wei Yin

Manufacturing Technology

Aalborg University

May 30ND 2025

AALBORG UNIVERSITY
STUDENT REPORT

The Faculty of Engineering and Science / Study Board of Mechanical Engineering and Physics
Fibigerstræde 16
DK - 9220 Aalborg Øst
Tlf. 99 40 99 40
snmp@mp.aau.dk / snp@mp.aau.dk
www.mp.aau.dk

English title:	Optimization of Gap Bridging Performance in Laser Butt Welding Using Beam Shaping Technology
Semester:	4. semester
Semester theme:	Master's Thesis
Project period:	February 2025 - May 2025
ECTS:	30 ECTS
Supervisors:	Morten Kristiansen
Project group:	VT4 Group 16
Participants:	

Wei Yin

Distribution:	1 pcs.
Page count:	43 pages
Appendix:	9pcs.

Abstract:

Autogenous laser butt welding is widely used for its high precision, low heat input, and efficiency. However, variations in joint gaps can degrade weld quality. The conventional solution—using high-precision fixtures—is costly, time-consuming, and limits production flexibility.
Beam shaping offers an alternative solution and can be classified into Dynamic Beam Shaping and Static Beam Shaping. Dynamic beam shaping, using High-Speed Scanning systems, provides high flexibility but is expensive and may cause melt pool instability at low frequencies. Static beam shaping, using Diffractive Optical Elements (DOEs), is cost-effective for large-scale production and easy to maintain but lacks adaptability for different tasks. This study, for the first time, applies Quasi-Static Beam Shaping using a Civan laser to design customized beam patterns for welding. The impact of these patterns on weld quality will be compared to conventional Gaussian beams, with melt pool behavior analyzed using high-speed and thermal imaging where possible. The goal is to determine an optimal beam shaping pattern and provide design insights for static beam shaping methods, particularly DOEs.

Preface

This thesis is part of the requirements for the Master's degree in Mechanical Engineering at Aalborg University.

Since the second semester of my studies, I have been conducting research under the supervision of Professor Morten Kristiansen, focusing on the application and principles of beam shaping in laser welding. The topic of this thesis represents a continuation and extension of the work carried out during the previous two semesters.

In the second semester, I began exploring how beam shaping techniques could enhance the gap bridging capability in the welding of ultra-thin tubes. This initial work laid the foundation for my understanding of welding experiment design and the fundamentals of laser welding. In the third semester, the research progressed to the use of advanced beam shaping technologies, such as Optical Phased Arrays (OPA) and Coherent Beam Combining (CBC), to generate custom beam profiles. These were investigated for their ability to control melt pool behavior and reduce welding defects. A cost-effective industrial solution for beam shaping was also proposed. Part of this research, specifically the work on controlling melt pool oscillations to reduce defects, was published as a conference paper titled *Beam Shaping to Control Weld Pool Oscillations* and will be presented at the 20th Nordic Laser Materials Processing Conference.

Through this experience, I gained deeper insights into melt pool dynamics and control theory in keyhole welding. Additionally, I designed a new beam measurement system based on the existing setup, making it suitable for high-power and long-focal-length laser systems.

The topic of this thesis was proposed under the guidance of Professor Morten Kristiansen, based on my prior research experience and the current industrial demand for improved gap bridging capabilities. The topic of this thesis was proposed under the guidance of Professor Morten Kristiansen, based on my prior research experience and the current industrial demand for improved gap bridging capabilities. The project was carried out in collaboration with Grundfos and involved the first-time use of Civan Lasers' highly flexible platform to systematically test dozens of beam patterns that influence the gap bridging capability.

Acknowledgements

I would like to express my heartfelt gratitude to my supervisor, Professor Morten Kristiansen, for his invaluable guidance and continuous support throughout this project. I am also deeply grateful for his help and encouragement throughout my entire Master's studies.

I would also like to thank PhD fellow Sebastian Ejlskov Schrøder for his technical assistance and insightful suggestions. My sincere appreciation goes to AAU laboratory technicians Kim Houtved Jensen and Søren Erik Bruun, whose support in sample preparation and fixture design was essential to the success of the experiments.

I would further like to thank my second-semester examiner, PhD Klaus Schütt Hansen, whose selfless advice helped shape my attitude towards research and academic growth.

I am especially thankful to Grundfos and to Jens Vestergaard Boll, Chief Technology Development Engineer at Grundfos, for his irreplaceable contributions to this project. Jens generously provided critical test samples, custom fixtures, access to analytical laboratory facilities, as well as technical guidance and valuable industrial insights throughout the third and fourth semester projects.

Finally, I would like to sincerely thank my parents for supporting my studies in Denmark, and my family, friends, and partner for their constant encouragement during this journey.

A special thanks goes to my girlfriend, Ms. Zihan Zhu, who is also a Master's student at Aalborg University. We met and fell in love during our time in Aalborg. Her unwavering support and encouragement throughout my studies have meant a great deal to me.

Contents

Introduction 1

Laser beam welding (LBW) is a Well-established but continuously advancing joining technique. It uses a focused laser beam as a heat source to melt the material at the joint, forming a molten pool that solidifies into a strong metallurgical bond [1]. Compared to traditional methods like flame or arc welding, laser welding offers a higher energy density, which result high efficiency, low distortion, and fine grain structure. it is also more user-friendly than electron beam welding, requiring less demanding environmental conditions. In addition, LBW can join a wide range of materials, including dissimilar materials, as long as they can absorb laser energy [2].

Due to these advantages, laser welding is widely used across industries from thin sheet components like ventilation ducts to large structures such as automotive bodies. On average, more than 60 meters of laser welds are used in each newly produced car [3]. According to industry reports, the global laser welding market is projected to reach approximately USD 3.6 billion by 2028, with a compound annual growth rate (CAGR) of 5.8% from 2023 to 2028 [4].

However, the same characteristics that make laser welding precise and efficient also make it highly sensitive to joint geometry. With typical beam diameters ranging from 10 to few hundred microns, even small misalignment or gap can lead to defects such as lack of fusion shows in Fig 1.1, because the laser beam can directly pass through the gap without heating the material [5]. Hight mismatches can distort the ennergy distribution due to laser beam' caustic shape, further affecting weld quality [3]. Therefore, precise joint tolerances are critical, especially in autogenous (Filler-free) welding. Meetig these tight tolerances often requires complex fixtures, increasing production costs, and reduce the flexibility of the production line [6].

Figure 1.1
Lack of fusion in 0.5mm gap duct welding

The effect of tolerances is different for different weld joints. Among joint types, the butt joint is one of the most commonly used configurations in welding applications. According to ISO9692-1:2013, it is formed by placing two workpieces end-to-end and welding along the seam [7]. This configuration is widely adopted for its material efficiency, good load-bearing characteristics, and suitability for both static and dynamic applications. Industries such as oil and gas, nuclear power, food processing, aerospace, and construction frequently use butt joints [8].

In particular, square-groove (non-beveled) butt joints are commonly used in laser welding due to the process's ability to achieve full penetration without filler material. This autogenous welding approach relies entirely on melting the base materials to form the joint, which improves chemical consistency in the fusion zone and eliminates the need for additional consumables. As a result, the process is simplified, enabling higher welding speeds and making it highly compatible with automation [9]. Despite these benefits, square-groove butt joints are particularly sensitive to

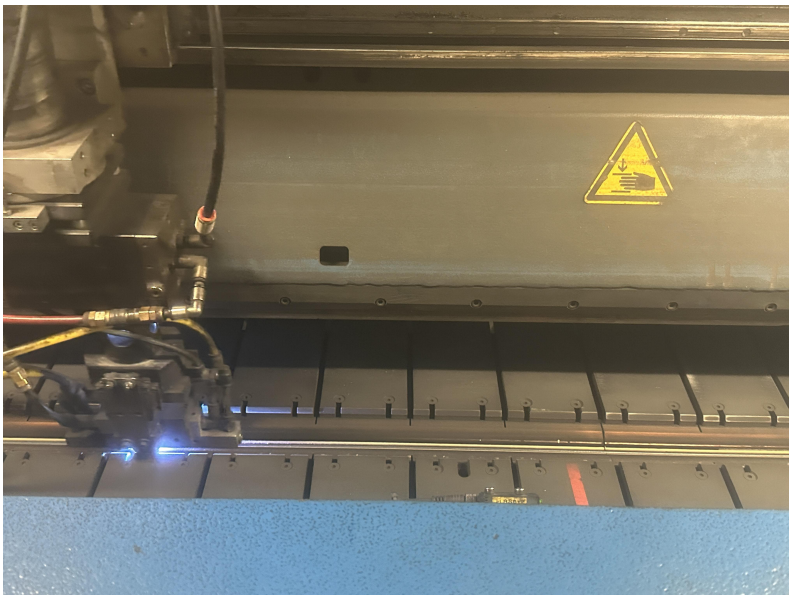

Figure 1.2
The automatic fixture of stainless steel pipe butt welding in JKF Industri

joint gaps, often requiring custom, high-precision fixtures and surface preparation [6, 10]. Figure 1.2 shows one such automatic fixture. While effective, these solutions are costly, inflexible, and often impractical for small-batch or multi-variant production, where frequent changes in part geometry occur [11].

An alternative strategy is to improve the laser's ability to tolerate gaps and variations in joint geometry. Enhancing this "gap bridging" ability would reduce the need for strict tolerances and complex fixtures, making the process more flexible and cost-efficient.

Therefore, improving gap bridging in laser butt welding is not only key to consistent weld quality but also vital for building flexible and automation-ready production systems. This leads to the central research question of this thesis:

how can the gap bridging capability in laser butt welding be improved?

Problem analysis 2

To effectively enhance the gap bridging capability in laser butt welding, it is essential to first understand the fundamental mechanisms of laser welding and the physical phenomena underlying gap bridging. In addition, a comprehensive review of existing techniques that have been developed to address this issue is required in order to identify their advantages, limitations, and research gaps.

This chapter begins by introducing the basic principles of laser-material interaction and the process dynamics involved in gap formation and bridging. It then reviews current strategies for improving gap bridging performance—such as filler wire addition and beam shaping—highlighting their mechanisms and constraints. Finally, the chapter identifies key unresolved scientific questions that form the basis for the present study.

2.1 The mechanism of laser beam welding and gap bridging

Laser beam welding (LBW) is a high-energy-density fusion welding process in which a focused laser beam is used as the heat source to melt and join metallic materials. The laser itself is a highly directional and coherent form of electromagnetic radiation, distinct from conventional light sources in both generation and behavior.

Laser principle

The term LASER is an acronym for "Light Amplification by Stimulated Emission of Radiation." The story of the laser first began with the concept of stimulated emission developed by Albert Einstein in 1916, and was first confirmed by experiments in 1928. Around 20 years later, the researchers realized for the first time the stimulated emission in a resonator system in the 1950s. The first laser was built by Maiman in 1960 which used ruby as a laser active medium and produced coherent and pulsed red light at a wavelength of 694 nanometers [12]. Three years later Korad and Raytheon promoted the first industrial laser for drilling processes in 1963, which Revealed laser technology has entered a rapid development stage. Today, laser has been applied to many area such as information transportation, medical application and material processing [13].

Fundamentally, three types of light–matter interactions can occur at the atomic level: *absorp-*

tion, *spontaneous emission*, and *stimulated emission* shows in Fig 2.1. Absorption occurs when photons interact with atoms or molecules in a lower energy state, promoting them to a higher energy state while photons disappear and absorbed by atoms or molecules. According to Planck, photons have quantized energy states, which means that the energy transfer is a multiple of the minimum quantized energy. This absorbed energy increases the internal energy of the material and is typically manifested as an increase in temperature [3].

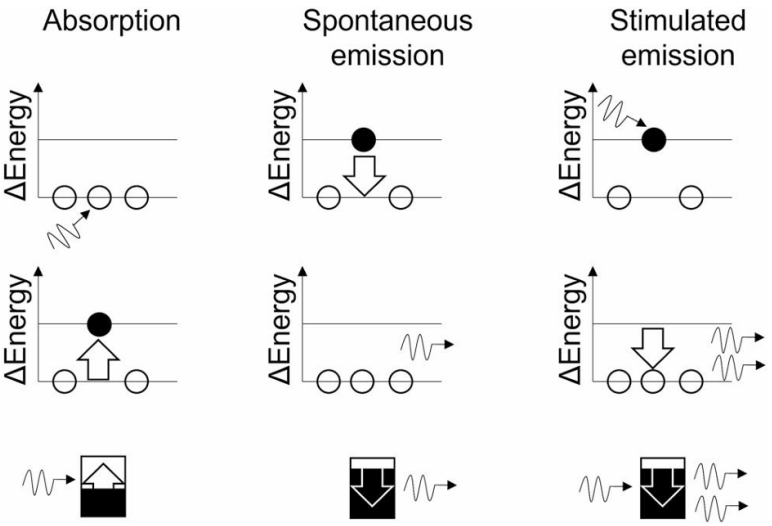

Figure 2.1
Three light-matter interactions, Reproduced from[3]

Spontaneous emission refers to the natural process by which excited atoms return to a lower-energy state, emitting photons in random directions, because most of attenuated states are unstable.

The third mechanism—stimulated emission—is the foundation of laser generation. When an excited atom is struck by a photon of matching energy, it releases a second photon with identical phase, wavelength, and direction. This process is also called relaxation of light, and the material containing excited atoms that are struck by photons and emit duplicate photons is known as the laser active medium (LAM). Therefore, the whole process can be seen as the amplification of light.

However, according to Boltzmann's law, the population of energy states in a system follows a distribution in which fewer atoms occupy higher energy states. This means that in regular materials at room temperature, most atoms are in the lower energy state (E_1), while only a few are in the higher energy state (E_2), as shown in Fig. 2.2. When a photon with matching energy illuminates the LAM, it is more likely to be absorbed, resulting in spontaneous emission rather than stimulated emission.

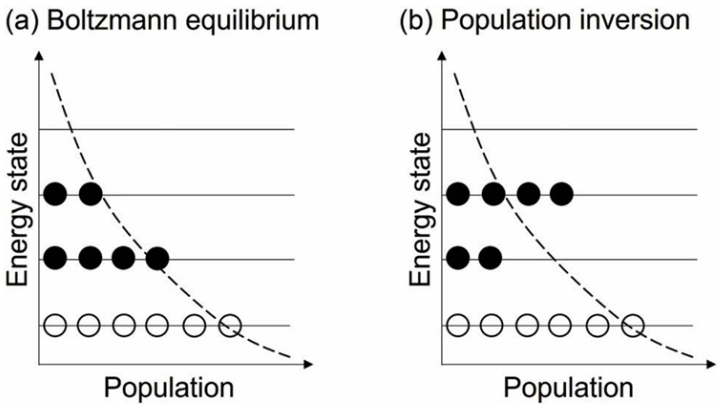

Figure 2.2
Principle sketch of population distributions at (a) thermodynamical equilib rium (Boltzmann equilibrium) and (b) population inversion, reproduced from [3].

Hence, Extra energy is necessary to be used to maintain the high population in excited energy which is named as population inversion, and the pumping was used to describe this process. Energy input can be achieved in different ways depending on the nature of the LAM; typical are optical pumping (absorption), electrical discharge (electron collisions), electric processes (semiconductors), or chemical processes. Most typical LAMs for lasers in production are solids and gases. Different combinations of arrangements form different lasers.

Unfortunately, the photon generated through stimulated emission at this stage is insufficient to constitute a coherent and collimated laser beam. To achieve sustained amplification and to spatially and temporally control the emitted photons, an optical resonator—typically composed of two parallel or concave mirrors positioned at either end of the Laser Active Medium (LAM)—is implemented. The resonator provides a well-defined optical feedback mechanism, wherein photons are reflected back and forth through the gain medium, stimulating further emission in phase and in the same direction as the initial photons. This process leads to constructive interference and exponential amplification of coherent radiation along the resonator axis.

In addition to facilitating light amplification, the optical resonator plays a critical role in defining the spatial characteristics and mode structure of the emitted laser beam. Through selective reinforcement of longitudinal and transverse optical modes, the cavity suppresses undesired spontaneous emission components and favors well-defined propagation patterns. In the ideal case, the stable resonator supports a fundamental transverse electromagnetic mode, TEM_{00}, characterized by a Gaussian intensity distribution. The Gaussian beam has special power distribution shows in equation.

$$I(r) = \frac{2 \cdot P_L}{w^2 \cdot \pi} \cdot e^{\frac{-2r^2}{w^2}}, \tag{2.1}$$

Although laser beams exhibit superior spatial coherence and directionality compared to conventional light sources, they are not perfectly collimated. Due to the wave nature of light and the diffraction-limited behavior of coherent beams, laser radiation inherently diverges as it propagates. This divergence gives rise to a characteristic beam geometry commonly described by the caustic diagram, as shown in Fig. 2.3, where w_0 denotes the beam waist radius—the minimum

radius of the beam—and z_R is the Rayleigh range, representing the distance over which the beam expands from w_0 to $\sqrt{2}w_0$. The spatial beam radius is conventionally defined as the radial distance from the beam center where the intensity drops to $1/e^2$ of its maximum value.

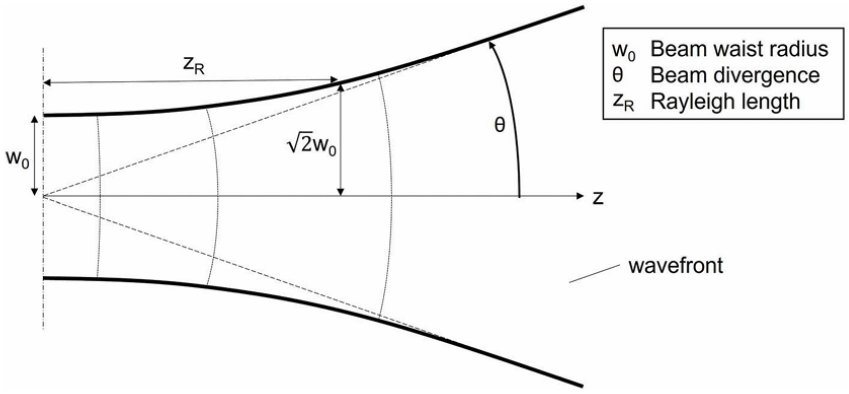

Figure 2.3
Laser beam propagation and caustic properties, reproduced from [3]

In practical laser systems, the ability of a beam to be focused to a small waist while maintaining low divergence is fundamentally constrained. This trade-off is quantified by the beam parameter product (BPP), defined as the product of the beam waist radius w_0 and the far-field divergence half-angle θ. For a perfect Gaussian beam, the BPP reaches its theoretical minimum of λ/π, where λ is the laser wavelength. However, real beams often deviate from this ideal case due to optical aberrations and higher-order transverse modes. These deviations are expressed by the beam quality factor M^2, such that

$$\text{BPP} = M^2 \cdot \frac{\lambda}{\pi}.$$

A lower M^2 value (closer to 1) indicates a beam that closely approximates a diffraction-limited Gaussian profile, with superior focusability and spatial coherence.

In industry application, Due to the caustic properties To enable efficient propagation and spatial control, the beam is first passed through a collimating lens to transform it into a near-parallel beam with minimal divergence. Following collimation, the beam is directed through a focusing lens to concentrate the optical power into a small spot. This step insure the high intensity in focus plane. Without collimation and proper focusing, the intrinsic divergence of the laser beam would result in reduced intensity and poor spatial resolution at the target. One of example shows in Fig2.4, Klaus et al. developed a HighYag laser head with DOE beam shaping, the beam caustic can be found before the collimation lens, after changing power distribution from Gaussian to Multiple spots by DOE, the beam was focused by certain focusing lens [14].

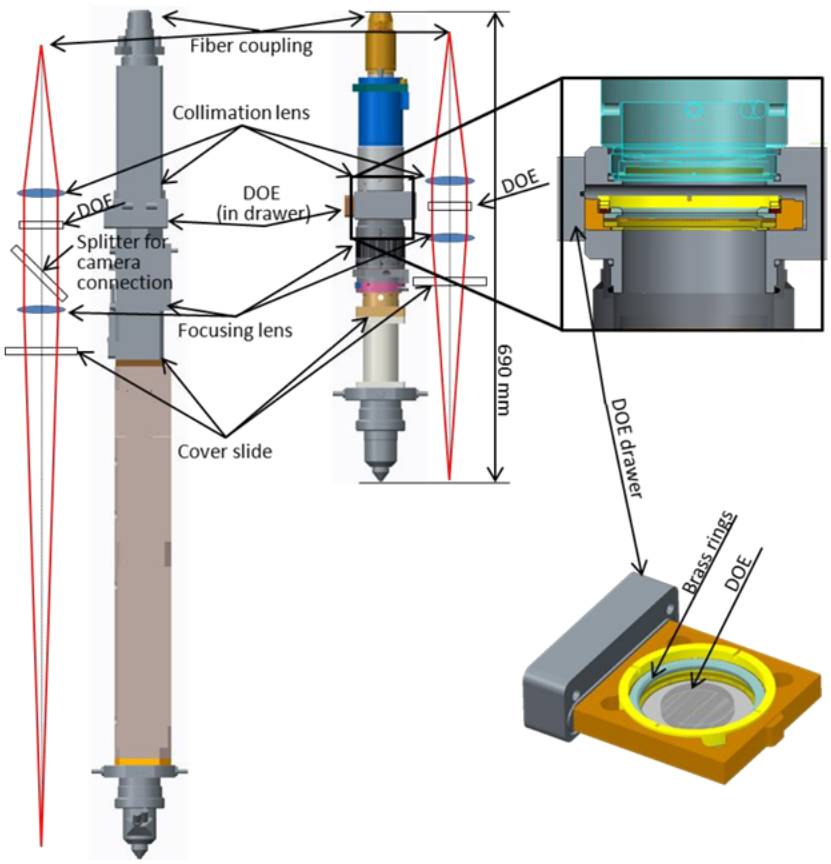

Figure 2.4
HighYAG laser head with DOE beam shaping and different focusing lenses designed by Klaus et al. Reproduced From [14]

By combining the three fundamental components of a laser system, namely the laser active medium (LAM), the pump, and the resonator, lasers with tailored characteristics can be engineered to meet diverse application requirements. Variations in these components allow control over critical beam properties such as wavelength, coherence, power, and spatial mode structure. Consequently, a wide range of laser types have been developed to fulfill the demands of different industrial and scientific tasks [3].

In general, laser beams have some characteries include high spatial and temporal coherence, narrow spectral bandwidth, and low divergence, and the energy carried by the photons in a laser beam is quantized and uniform enable the generation of tightly focused spots with high energy density. In laser welding applications, the focused beam radius at the working plane typically ranges from $50\,\mu m$ to $200\,\mu m$, depending on the optical system and beam quality [15]. and the fundamental transverse electromagnetic mode TEM_{00} or a near-Gaussian intensity distribution is commonly used, In some of high-power industrial systems, beam shaping or multimode delivery also be applied to improve process robustness.

Laser beam energy transfer

One of the most critical mechanisms in laser welding is the transfer of energy from the laser beam to the material. As discussed in the previous subsection, the laser beam carries a high amount

of energy, which can be concentrated through focusing to achieve the necessary energy density for welding. When the laser beam irradiates the surface of the workpiece, three fundamental interactions can occur—absorption, reflection, and transmission [3]—as illustrated in Fig. 2.5.

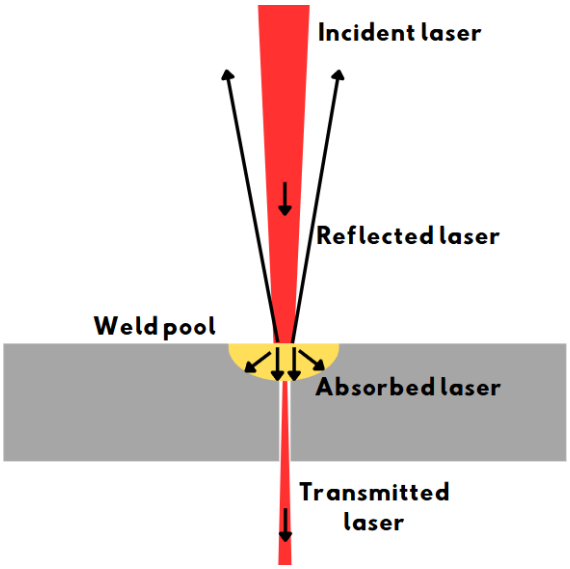

Figure 2.5
Three Laser mechanisms

Absorption refers to the interaction between the laser photons and the solid or liquid surface (or in some cases, the plasma volume), resulting in the partial conversion of optical energy into thermal energy. while the photonic energy is assumed to be first transferred to the electrons that increase the energy state of the system. Afterward, the electron energy is transferred to the atom and the lattice, where heat conduction takes place in the form of particle collisions that transfer momentum and thereby energy. This absorbed heat drives the thermodynamic processes essential for welding. The absorptivity is defined as the ratio of energy absorbed by the workpiece to the total incident laser energy, and it depends on several factors, including the laser wavelength shows in Fig 2.6, angle of incidence, material properties, surface conditions, joint geometry, and welding mode. Notably, the absorptivity can vary significantly during the welding process. For example, in keyhole welding, the absorptivity increases after a stable keyhole is formed due to multiple internal reflections within the narrow and deep structure. In contrast, conduction mode welding generally exhibits lower absorptivity due to the absence of such confined geometries [3, 16].

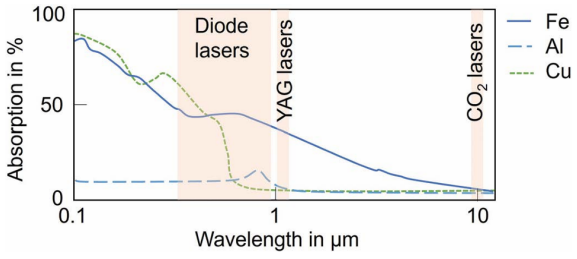

Figure 2.6
Wavelength-dependent absorptivity of different materials at room tempera ture and perpendicular laser beam illumination, Reproduced from [3]

Reflection occurs when a portion of the incident laser is redirected away from the surface of the solid or liquid material. Reflected laser energy can potentially return to the optics of the laser head, causing thermal or optical damage. Therefore, in industrial practice, the laser head is typically positioned at a certain angle to reduce the risk of back-reflection [17]. In addition, reflected beams can pose safety hazards to surrounding equipment and personnel, which is why laser welding must be carried out with appropriate safety shielding, in accordance with ISO 11553-1 standards [18].

Transmission includes both optical and thermal transmission mechanisms. Optical transmission occurs when the laser passes through a transparent or semi-transparent material without significant absorption, or when it penetrates through an open gap without interacting with the workpiece. Thermal transmission, on the other hand, is often observed during high-power keyhole welding. When the keyhole depth exceeds the material thickness, energy can escape through the bottom surface of the workpiece in the form of direct laser radiation or vaporized material.

In general, among these three mechanisms, absorption is the most desirable in laser welding, as it directly contributes to energy utilization and process efficiency.

Melt pool behavior and flow dynamics in laser welding

Laser welding is a dynamic process in which the laser-induced molten pool—and, in some cases, a keyhole—moves relative to the workpiece, resulting in the formation of a continuous weld seam that joins multiple components. Depending on the peak energy density delivered by the laser, two primary welding modes can occur: conduction mode and keyhole mode.

When the power density at the workpiece surface is below approximately $1 \times 10^6\,\mathrm{W/cm^2}$ in 1064nm Nd:YAG laser with stainless steel, laser welding typically occurs in conduction mode, where heat is transferred primarily through thermal diffusion [19]. In this regime, a quasi-steady-state energy balance is achieved, wherein the absorbed laser energy is offset by losses due to heat conduction, thermal radiation, and latent heat during melting. Radiative and evaporative losses are generally negligible compared to conductive losses. Classical heat conduction models can be used to estimate the weld penetration depth Z. In conduction mode, the weld geometry is determined by conductive heat transfer and melt flow within the pool [3].

The flow behavior in the melt pool is primarily governed by thermocapillary (Marangoni) convection and buoyancy effects, both of which are driven by thermal gradients. Due to thermal expansion, the density of molten metal decreases with increasing temperature. In a typical laser melt pool, the temperature is highest near the center and decreases toward the pool boundaries, leading to a density gradient. The lighter (hotter) fluid tends to rise, while cooler, denser fluid sinks, generating buoyancy-driven flow. Meanwhile, surface tension generally decreases with increasing temperature. This causes molten metal to flow from regions of low surface tension (hotter) to high surface tension (cooler), a phenomenon known as Marangoni flow. The direction and magnitude of this flow depend strongly on the temperature coefficient of surface tension, which in turn may be influenced or even reversed by the presence of specific alloying elements

or surface-active species [3], Shows in Fig 2.7.

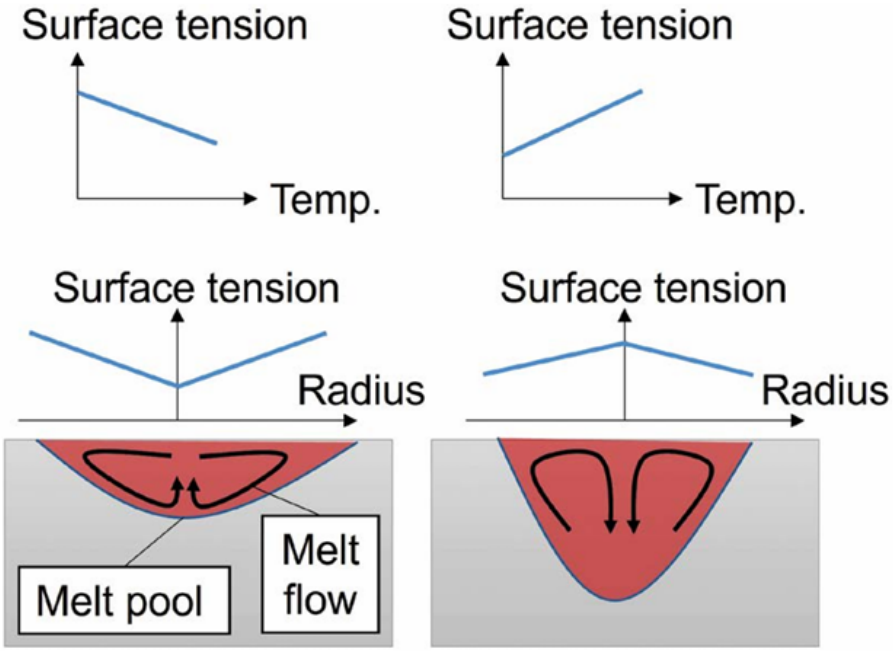

Figure 2.7
Surface tension dependence of the Marangoni flow[3]

When the energy density exceeds approximately $1 \times 10^7\,\mathrm{W/cm^2}$ in 1064nm Nd:YAG laser with stainless steel, keyhole mode welding is initiated. In this regime, the melt pool and flow dynamics are fundamentally altered. Under quasi-steady-state conditions, the moving keyhole absorbs a substantial amount of energy through multiple internal reflections, leading to sustained evaporation of material and the generation of recoil pressure. This recoil pressure maintains the keyhole's open geometry and drives intense fluid flow within the molten pool [20].

The melt pool geometry, defined by the liquid–gas interface at the keyhole, the solid–liquid boundaries of the melting and solidification fronts, and the free surface, is influenced by both conductive heat transport and forced convection. The relative motion between the laser beam and the workpiece introduces additional flow components. As illustrated in Fig. 2.8, a quasi-steady-state keyhole exhibits complex internal circulation patterns. Unmelted metal at the front of the keyhole is heated and melts, while molten metal is accelerated and pushed toward the trailing edge [17].

Since only a small fraction of the molten material is lost through evaporation at the keyhole front, mass conservation requires the redistribution of molten metal from the front to the rear of the keyhole. This redistribution is facilitated by the combined effects of recoil pressure and weld travel speed. The molten metal is accelerated past the keyhole and directed toward the rear, where it solidifies to form the weld seam. These mechanisms are shown as flow patterns A and G in Fig. 2.8, as described in [17].

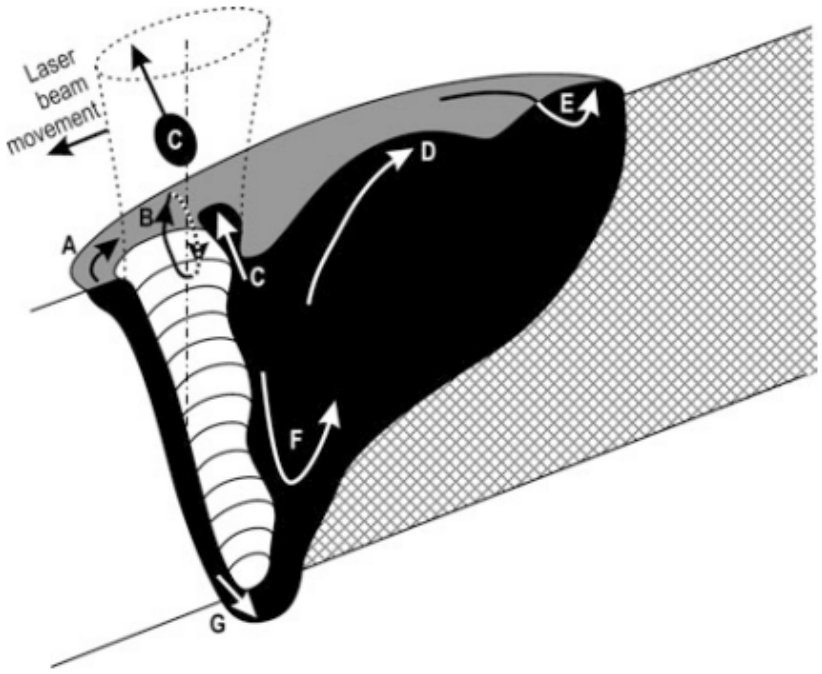

Figure 2.8
Different melt flow phenomena during laser welding. Reproduced from [17].
A. *Melt flow redirected to pass around the keyhole.*
B. *Marangoni flow driven by surface tension gradients.*
C. *Redirected flow that can cause spatter.*
D. *Humping caused by accumulating downstream flow.*
E. *Stagnation point for accelerated flow.*
F. *Inner eddies.*
G. *Keyhole front melt film flow downwards.*

Gap bridging principle

Gap bridging in autogenous laser welding is a complex, multi-physical phenomenon that involves rapid heating and cooling, dynamic melting and evaporation, melt pool convection, solidification, and non-equilibrium phase transformations[21]. Despite its practical significance, the fundamental mechanisms behind gap bridging remain insufficiently explained in standard welding textbooks. Given its excellent mechanical properties and widespread use in aerospace applications [22], Ti-6Al-4V is often used as a representative material in gap bridging studies[23–25], particularly due to the prevalence of thin-walled structures in such fields[26].

Most studies investigating gap bridging mechanisms employ coupled CFD models to simulate melt pool behavior under varying gap conditions, followed by experimental validation [27]. Both pulsed and continuous wave laser sources have been studied. For example, Duan et al. developed a numerical model to simulate the melt pool dynamics during autogenous laser welding of Ti-6Al-4V with variable gap widths. Using a 2 mm thick Ti-6Al-4V plate, they explored linear gap variations from 0 mm to 0.4 mm under a continuous-wave laser of 1350 W power and 30 mm/s welding speed [28].

Their results shows in Fig 2.9 indicate that, at the initial stage of welding, a keyhole is rapidly formed at the laser focus, resulting in a small melt pool with steep thermal gradients. Driven

by Marangoni convection, the molten metal around the keyhole flows outward, expanding the pool and forming a preliminary liquid bridge. At around 50 ms, the melt pool enters a quasi-steady state, where surface flow toward the trailing edge becomes evident. Simultaneously, some molten metal is pushed toward the front edge of the keyhole due to recoil pressure and shear forces from vapor jets, forming a forward liquid bridge that partially spans the gap. This behavior resembles—but is distinct from—the flow pattern A described in Fig. 2.8.

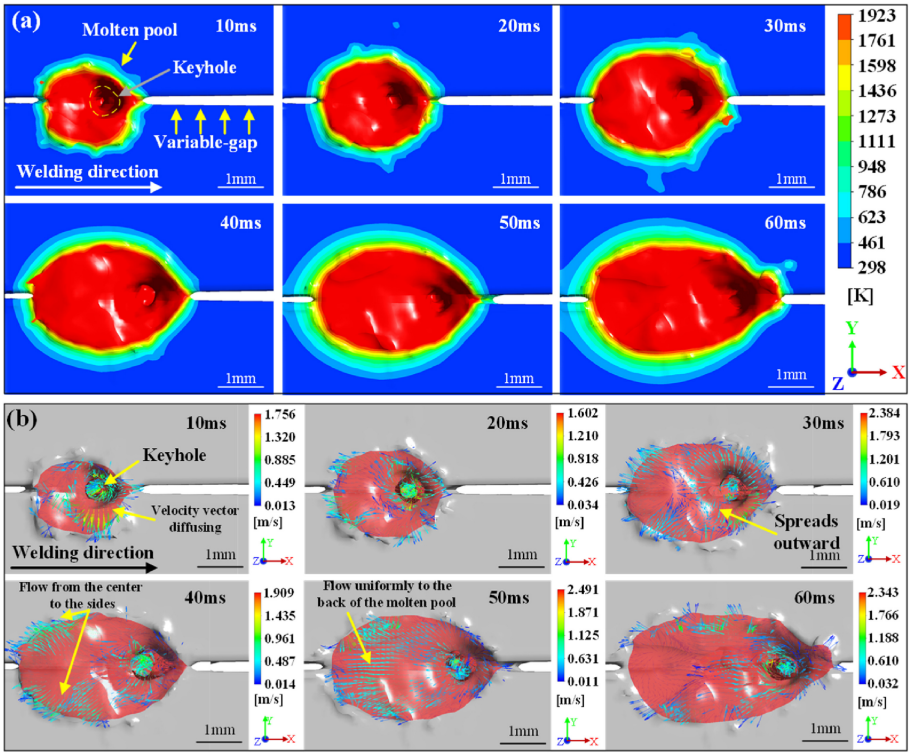

Figure 2.9

Simulation of temperature(a) and fluid fields(b) in autogenous gap welding, Reproduced from [28]

As the gap widens to 0.2 mm at around 60 ms, the melt pool adapts: molten metal flows inward from both sides toward the center to fill the larger gap. The authors also analyzed the 3D melt pool shape under steady-state conditions, shows in Fig 2.10. When the gap is smaller than 0.2 mm, the pool geometry closely resembles that of a zero-gap condition. However, as the gap increases, the keyhole depth decreases, the melt pool becomes more dynamic, and its bottom width expands. The latter may be related to enhanced heat transfer in the presence of entrapped air at the gap region.

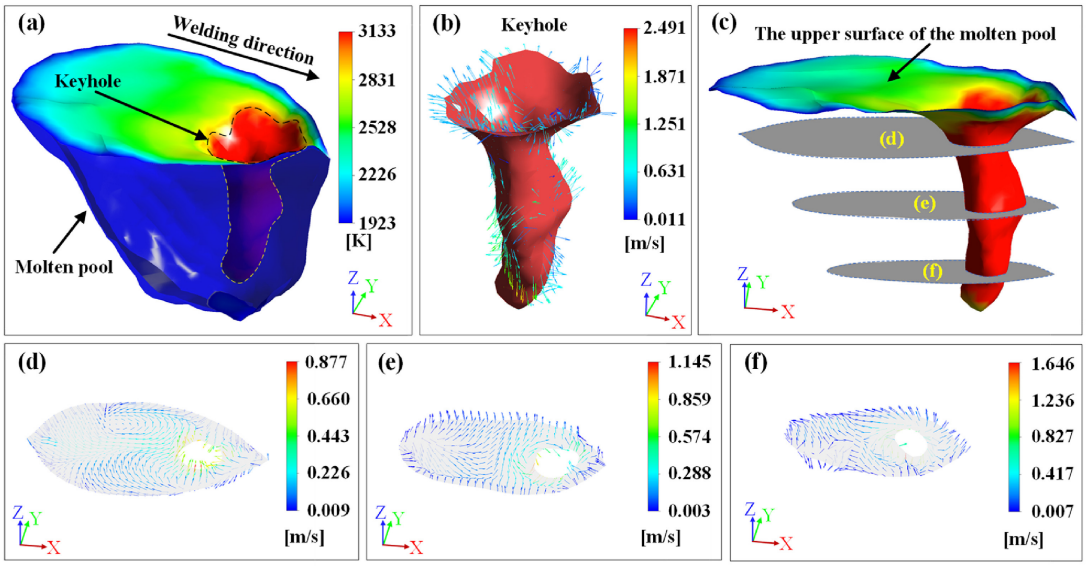

Figure 2.10

Keyhole characteristics in stable welding process: (a) keyhole position; (b) Velocity distribution; (c) Location of internal velocity distribution section; (b–d) Flow field distribution of the corresponding section, Reproduced from [28]

Overall, the study suggests that gap bridging involves two primary mechanisms. First, forward liquid bridges form due to keyhole-induced frontward melt flow driven by recoil pressure and vapor dynamics. Second, rearward bridging occurs via inward melt flow from the sides and back, which eventually solidifies into the weld seam. The vertical height difference between the weld center and the base material can serve as a quantitative indicator of gap bridging quality: smaller height differences imply better bridging. Building upon the previous work, Jicheng Chen et al.

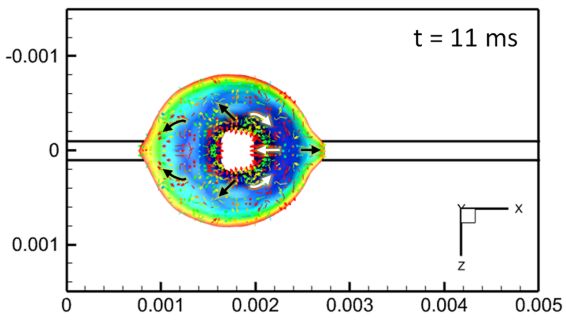

Figure 2.11

Spatter on surface

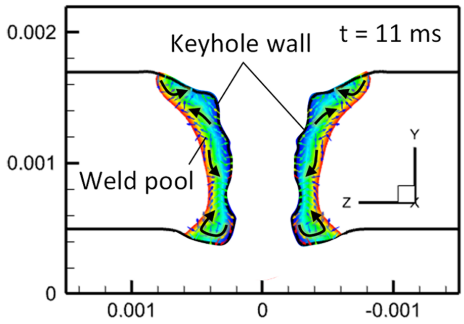

Figure 2.12

Automatic laser welding

[25]. conducted a numerical simulation of pulsed laser welding with uniform joint gaps of 0.2 mm, 0.3 mm, and 0.4 mm, using a comparable CFD-based modeling approach. In their study, a top-hat beam profile with a diameter of 700m was employed, operating at a peak power of 2400 W, a pulse frequency of 20Hz and a pulse duration of 30 ms. The welding speed was maintained at 30mm/s, consistent with the previous continuous laser study.

As shown in Figs. 2.11 and 2.12, when the gap was 0.2mm, the melt pool behavior during the laser-on phase resembled that observed in continuous wave (CW) welding (cf. Fig. 2.9), featuring a well-defined keyhole and a forward liquid bridge. However, once the laser pulse was terminated, the keyhole rapidly collapsed due to a significant drop in temperature along the cavity walls, and

the melt pool volume decreased. Within approximately 10ms, the molten metal solidified, forming a strong bridge over the joint gap. When the subsequent laser pulse arrived, the previously formed weld spot was remelted, and a new liquid bridge was immediately formed at the front of the melt pool. Due to thermal accumulation effects, the surface melt pool became significantly elongated. At the end of the second pulse, a noticeable residual liquid volume was still present, indicating incomplete solidification.

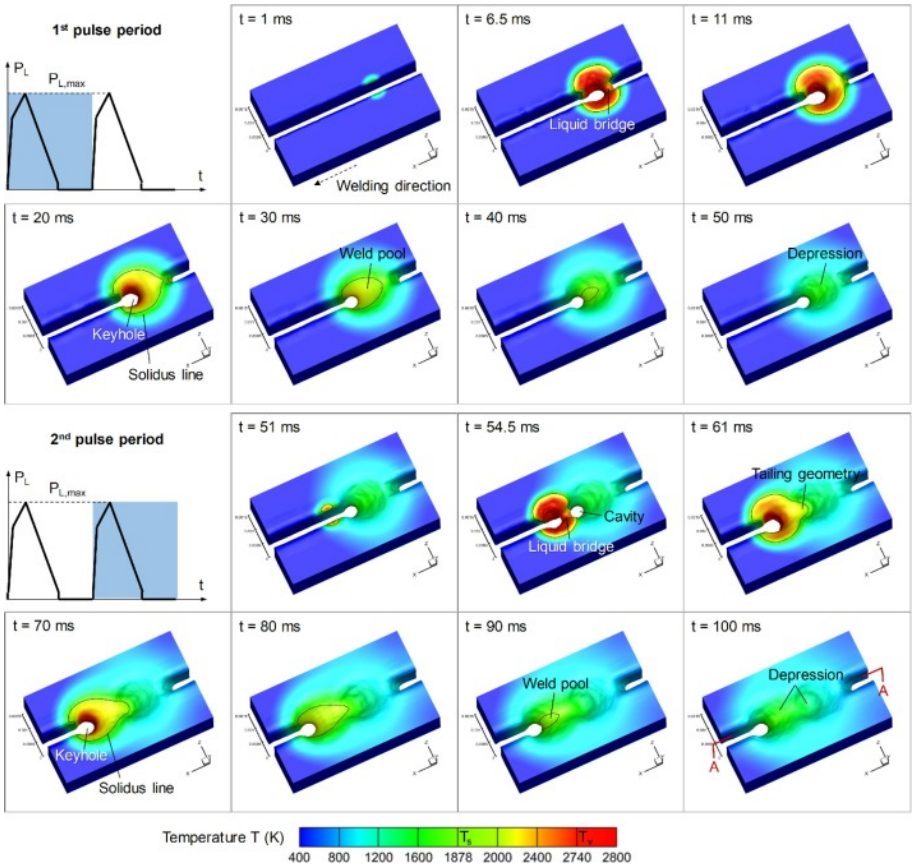

Figure 2.13

Evolution of temperature field and phase interface within the initial two pulse periods under a reserved clearance size of 0.4 mm, Reproduced from [25]

Fig. 2.13 illustrates the melt pool morphology at a gap size of 0.4mm. In this case, the forward liquid bridge was no longer observed, and bridging occurred only at the trailing edge of the beam. Furthermore, the absence of a visible keyhole suggests that part of the laser beam passed directly through the joint gap, significantly reducing the energy utilization and welding efficiency. The melt pool behavior shifted from being dominated by recoil pressure and hydrostatic pressure, as seen in smaller gaps, to being governed primarily by surface tension forces.

In summary, when the joint gap exceeds a critical size, the welding process transitions away from the keyhole mode, and no forward liquid bridge is formed. Instead, gap bridging relies solely on the lateral melting of the joint edges, followed by the inward flow of molten metal under the influence of gravity and surface tension. Compared to keyhole-mode welding, this bridging mechanism involves a reduced amount of molten metal, leading to a lower capacity to compensate for larger gaps.

2.2 Methods for improving gap bridging in laser welding

In order to improve the gap bridging capability and ensure weld quality, a wide range of techniques have been developed. This section reviews and categorizes these approaches based on their operating principles and applicability.

Wire feeding is one of the earliest methods proposed to enhance gap bridging. As early as 1999, Sun et al. [5] introduced wire feeding into Nd:YAG laser welding to successfully bridge a 1.0 mm gap in 2 mm-thick stainless steel sheets. Wire feeding provides additional molten metal to fill the joint gap. Later in 2010, Aalderink [29] performed welding experiments on 1 mm thick AA5182 aluminum sheets and quantified the improvement: gap bridging could be achieved up to 50% of the sheet thickness with wire, compared to 33% without. In the same year, Salminen [30] suggested that for high-quality welds, the allowable gap should remain under 10% of the material thickness.

To enable stable welding under larger joint gaps and improve performance on reflective materials, hybrid welding methods such as laser-MIG welding have been developed [31]. By providing an auxiliary heat source and additional filler at the top of the melt pool, these methods allow successful welding of joint gaps up to 2.5 mm. Laser beam oscillation has also been integrated with wire feeding to mitigate alignment errors and improve robustness [32]. However, due to structural constraints and post-weld processes, wire-based strategies may not be suitable in some industrial applications [23].

Alternatively, **autogenous laser welding**—which relies solely on melting the base material without filler wire—has also been studied as a means of gap bridging. By eliminating the need for wire feeding equipment, autogenous welding can simplify system design, reduce parameter sensitivity, and potentially improve efficiency. Most techniques aiming to improve autogenous gap bridging focus on **laser beam energy manipulation**, which can be divided into two main categories: temporal shaping (e.g., **pulsed wave laser beam welding, PWLBW** [33]) and spatial shaping (i.e., **beam shaping** [11, 34, 35]). Recent works have attempted to combine both methods into hybrid approaches [23, 24].

However, despite the advantages of PWLBW in certain contexts, this approach suffers from several drawbacks, including lower welding efficiency, unstable keyhole behavior, susceptibility to porosity or cracking, high equipment cost, and a narrow process window. Since the current study aims to identify promising gap-bridging strategies suitable for industrial applications, wire-based methods and pulsed welding will not be pursued further. Instead, beam shaping techniques will be examined in detail in the following section.

2.3 Beam shaping for enhanced gap bridging

Beam shaping refers to the technique of redistributing the spatial or temporal energy profile of a laser beam to achieve improved process stability, energy coupling, and melt pool control [36]. Several distinct methods of beam shaping have been proposed and evaluated in the context of laser welding, particularly for enhancing gap bridging capability.

One widely used static beam shaping method is based on Diffractive Optical Elements (DOEs), which modulate the laser wavefront through precisely engineered microstructures. As shown in Fig. 2.4, DOEs can be easily integrated into laser optics, enabling quick replacement to produce various beam profiles without requiring active components or frequent maintenance. DOEs are generally categorized into three types: DOE splitters, which replicate the original beam into multiple spots and are ideal for multispot welding; DOE shapers, which generate simple patterns like ellipses or rings with relatively high efficiency; and DOE diffusers, which can project arbitrary patterns at the expense of optical efficiency [37].

In the context of gap bridging, Hanse et al. [38] employed a DOE-based splitter to create a multispot configuration for butt joint welding, demonstrating that the weld seam width increased, thereby improving gap tolerance. Similarly, Volpp et al. [34] used a 2x2 multispot array generated by DOE to form four separated keyholes, which led to better gap bridging than single-spot welding. This was attributed to the altered melt flow: energy peaks near the beam spots induced localized keyholes and drove molten metal toward the joint gap center. On this basis, Kristiansen et al. [35] developed a 9-spot beam to simultaneously weld four sheets in a lap configuration. However, DOE methods are inherently limited by their static nature, requiring pre-fabricated designs for each beam pattern, making them less flexible for adaptive control. Moreover, most existing studies focus on simple multispot configurations rather than customized intensity patterns.

A dynamic alternative is the use of oscillating laser beams, also known as beam wobbling. In this method, galvanometer mirrors or piezo-driven optics scan the beam along predefined 2D or 3D paths (up to 10 kHz), modifying the spatial energy distribution. This approach has been shown to suppress melt pool defects [36], widen the process window [39], and improve gap bridging in autogenous welding [40]. However, challenges remain. High oscillation frequencies often reduce effective amplitude, limiting control precision. Even state-of-the-art systems may be too slow to ensure stable melt pool dynamics, potentially increasing turbulence and instability. Furthermore, the high cost and complexity of these systems pose barriers for widespread industrial deployment.

Recently, deformable mirrors—originally developed in astronomy for adaptive optics—have been adapted for real-time beam shaping in high-power laser welding. These mirrors can modulate the beam shape at up to 100 Hz. Mi et al. [11] generated elliptical beam profiles using a deformable mirror to enhance energy coupling in butt joint welding with varying gap sizes. The short axis of the ellipse was aligned along the welding direction to maximize material interaction. Compared to Gaussian beams, the shaped beam demonstrated significantly better gap bridging. The tech-

nology holds promise for integration with machine learning–based weld monitoring and control systems [41]. However, deformable mirrors are still expensive and require active maintenance, which limits their industrial scalability.

In addition to the above techniques, several emerging methods have potential for enhancing gap bridging but have not yet been widely studied in butt joint applications. These include dual-clad fiber beam shaping, where two independently modulated power levels are coupled into the fiber core and inner cladding. This method has been shown to improve melt pool stability [42]. Ring-mode adjustable fiber lasers have also been used to tailor power distributions between the core and ring, enabling more stable keyhole formation and increased openness [43]. Another advanced technique is coherent beam combining (CBC) using optical phased arrays (OPA), where multiple low-power beams are amplified and recombined into a high-power beam with programmable 2D profile, focus, and position at MHz frequencies [44, 45]. While this method enables real-time control of beams exceeding 16 kW, its high cost, complexity, and large physical footprint currently hinder its deployment in production environments. As a potential industrial solution, Wei [46] proposed using OPA-CBC for experimental optimization of beam profiles and weld parameters, followed by implementation of static DOEs designed based on the optimized pattern for scalable manufacturing.

2.4 Limitations in previous studies

Although various beam shaping techniques have demonstrated improved gap bridging performance in laboratory-scale experiments, several limitations hinder their industrial applicability. Many of the proposed solutions rely on bulky equipment, involve high implementation and maintenance costs, and require complex integration, making them unsuitable for high-throughput or cost-sensitive manufacturing environments. To date, no mature beam shaping solution has been specifically developed with industrial deployment as its primary objective.

Moreover, most existing studies have focused on evaluating the overall effectiveness of specific beam shaping methods in enhancing gap bridging. However, there remains a lack of systematic investigation into how different spatial energy distributions—independent of the shaping technique—affect the gap bridging mechanism and lack of error analysis in real welding. This limits the generalizability and design flexibility of current approaches.

Finally, the fundamental physical mechanisms through which shaped beams contribute to improved gap bridging, such as altered melt pool dynamics, keyhole behavior, and surface tension-driven flows, remain insufficiently explored. A deeper understanding of these phenomena is essential to develop adaptive and robust beam shaping strategies for real-world applications.

2.5 Proposed solution for industrial gap bridging

To address the limitations identified in Section 2.4, this study proposes a novel beam shaping strategy that combines the advantages of different shaping technologies. Diffractive Optical Elements (DOEs) offer excellent compatibility with existing production lines due to their compact form factor, high efficiency, and minimal maintenance requirements. These characteristics make DOEs highly suitable for large-scale industrial applications. However, the major drawback of DOE-based systems lies in their lack of flexibility: the beam pattern is fixed during manufacturing, and the design and fabrication process requires prior knowledge and is time-consuming.

In contrast, Optical Phased Arrays (OPA) and Coherent Beam Combining (CBC)-based beam shaping offer exceptional flexibility and dynamic control. Their high modulation frequency enables quasi-static beam shaping that can emulate the effects of DOE-like patterns. More importantly, these systems can be used for extensive pre-experiments to optimize beam profiles and welding parameters. The data obtained can then be used to design and manufacture custom DOEs for specific production tasks.

Advantages of the proposed strategy:

- **Low-cost retrofitting:** Some of existing production lines can be modified with minimal changes by inserting DOEs into the collimated beam path.
- **Faster customization:** OPA-assisted development significantly reduces the design and validation time of DOEs, enabling rapid deployment of optimized beam shapes.
- **Cost-effective operation:** Once implemented, DOEs operate passively with no need for power or control systems, resulting in very low long-term operating costs.

Limitations of the proposed strategy:

- **Thermal sensitivity:** When inserted directly into high-power Gaussian beams, DOE components may experience refractive index shifts and deformation due to thermal gradients.
- **Lack of adaptiveness:** Static beam profiles are less effective for highly variable joint geometries, especially compared to AI-driven dynamic shaping systems capable of real-time adaptation.
- **Manual reconfiguration:** In production environments requiring frequent beam pattern changes, manual DOE swapping can reduce efficiency and increase downtime.

Problem statement 3

As discussed in Chapter 2, among the various approaches for improving gap bridging performance, autogenous laser welding assisted by beam shaping technologies presents the greatest potential for industrial application. While a range of beam shaping methods—such as DOEs, beam oscillation, deformable mirrors, and optical phased arrays (OPA)—have been developed and validated under laboratory conditions, most of these efforts have prioritized technological demonstration over industrial scalability.

Moreover, previous studies have largely focused on comparing shaping techniques as a whole rather than systematically investigating how specific laser beam profiles affect gap bridging capability. In particular, limited attention has been paid to understanding the underlying physical mechanisms linking energy distribution to melt pool dynamics in the context of gap bridging. Existing DOE-based research has predominantly relied on simple multiple-spot configurations without optimizing the spatial profile for different joint conditions.

To address this gap, a hybrid strategy has been proposed that leverages OPA systems for rapid beam profile prototyping and DOE design optimization. However, due to the lack of in-house manufacturing capabilities for static optical elements, this study focuses exclusively on the use of dynamic shaping via a Civan Laser system to emulate DOE-like patterns and evaluate their effect on welding performance.

This leads to a crucial scientific inquiry:

> *How do different laser beam profiles influence gap bridging capability in autogenous butt welding, and what physical mechanisms underlie their effectiveness?*

Solution 4

In response to the challenges identified in Chapter **??**, this chapter outlines a practical solution strategy aimed at enhancing the robustness of laser welding by improving gap bridging capabilities through beam shaping technologies. The approach centers on applying experimental methods to systematically investigate and address the core issues.

4.1 Test conceptualization

Guided by the existing infrastructure in the AAU Flexible Laser Processing Laboratory, the experimental strategy focuses on the following objectives:

1. To assess the effects of different beam patterns on the ability to bridge gaps during welding.
2. To identify the physical mechanisms by which energy distribution influences gap bridging.
3. When feasible, to evaluate how joint geometric tolerances negatively affect bridging performance in realistic welding scenarios.

A summary of the currently available laboratory resources is provided in Table 4.1. These resources serve as the foundation for the experimental design proposed in the following sections.

The most critical equipment used in this study is the Civan DBL fiber laser, which enables the rapid design and testing of various beam profiles. Combined with a custom-built conveyor system, welding experiments can be performed at speeds up to 100 mm/s. The process is coordinated through an in-house PLC control program, allowing synchronized control of the laser output and sample motion.

The laboratory is also equipped with an infrared thermal camera and a high-speed imaging system, which can be used to investigate the underlying mechanisms behind the influence of beam profiles on gap bridging performance. However, as the high-speed camera will not be available until after May 30, this report will not include results related to that part of the investigation.

In all experiments, 2 mm-thick 304 stainless steel sheets are used as the base material due to their good weldability, moderate cost, and wide range of industrial applications. Research focused on 304 stainless steel has strong industrial relevance, especially in cost-sensitive sectors.

The available machining resources at AAU are utilized to manufacture simple customized fixtures and to prepare weldable sample plates. Finally, due to the current limitations in analysis equip-

ment—primarily a microscope and a set of metallographic preparation tools—the weld quality assessment is restricted to destructive cross-sectional evaluation. According to ISO 13919-1 standards, the bridging performance is evaluated by measuring the height offset between the weld seam and the adjacent workpiece surface [47].

Table 4.1
Summary of Available Laboratory Resources

Section	Category	Equipment / Resource	Function / Notes
Primary Experimental Resources			
Laser System	Laser System	Civan DBL Fiber Laser (14 kW, 1500 mm focal length)	Core heat source with beam shaping capability
	Laser Mounting	KUKA Quantec Robot Arm (Industrial-grade robot)	Provides programmable laser positioning
	Motion Platform	Custom Conveyor System (Lab-customized conveyor)	Controls sample motion under laser
	Control System	Custom PLC Control Program (Laser and conveyor synchronized control)	Synchronizes motion and laser firing
	Thermal Monitoring	IR 8380 Thermal Camera with IR Filters	Captures thermal data during welding
	Imaging System	High-speed Camera (Model unknown, unavailable before May 30)	For melt pool/spatter observation
	Sample Materials	2mm 304 Stainless Steel Plates	Base material for welding experiments
	Shielding Gas	Nitrogen Gas Nozzle and Supply	Maintains inert welding atmosphere
Machining Resources			
CNC Equipment	CNC Machine	CNC 5-axis Machine	Enables precision fixture manufacturing
Cutting Equipment	Metal Cutter	HoAN Cut Machine (For sheets <4 mm)	Used for cutting metal sheets
Cutting Equipment	Laser Cutter	Laser Cut Machine	Fabricates custom welding samples
Experimental Analysis Equipment			
Microscopy	Microscope	Zeiss Microscope with Coaxial Camera (Movable platform included)	Microscopic analysis of welds
Metallurgical Testing	Metallography Kit	Full Set of Metallographic Testing Equipment	Evaluates weld morphology and quality

The experimental procedure is divided into two main stages:

1. Beam Pattern Screening: In the first stage, a series of beam patterns will be tested to compare their gap bridging performance. Several representative welding parameters will be selected to evaluate how different beam shapes perform under varying process conditions. A variable-gap butt joint method will be employed, as illustrated in Figure 4.1, this set-up has

been proven in Hanxuan et.al's research [31]. In this setup, the initial gap starts at 0 mm and gradually increases to 1 mm at the end of the joint. After welding, the maximum bridged gap width for each beam pattern can be quickly assessed, providing a preliminary indication of its bridging capability. Based on these results, a few representative beam profiles will be selected for further analysis. Cross-sectional examinations will then be performed on welds produced under different fixed gap widths to evaluate welding quality and bridging performance.

2. Mechanism Investigation: In the second stage, a fixed-gap joint configuration will be used (see Figure 4.1) to enable a steady-state observation of melt pool dynamics. High-speed imaging and infrared thermography will be employed during welding to capture the evolution of the melt pool. Selected beam patterns from the first stage will be tested under several fixed-gap conditions to explore the underlying physical mechanisms that govern gap bridging behavior.

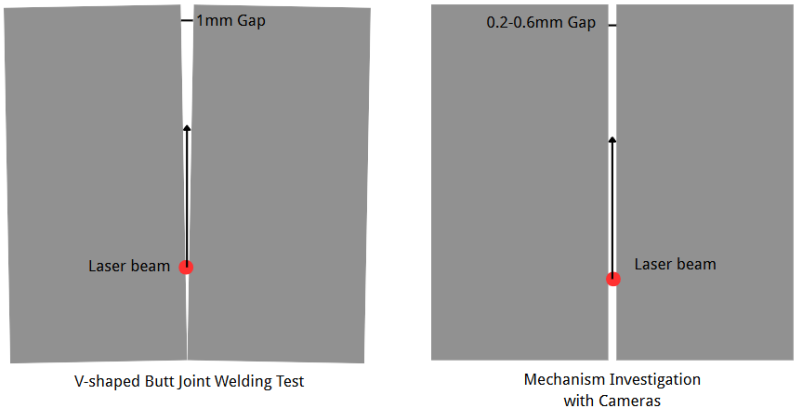

Figure 4.1
Variable gap and fixed gap

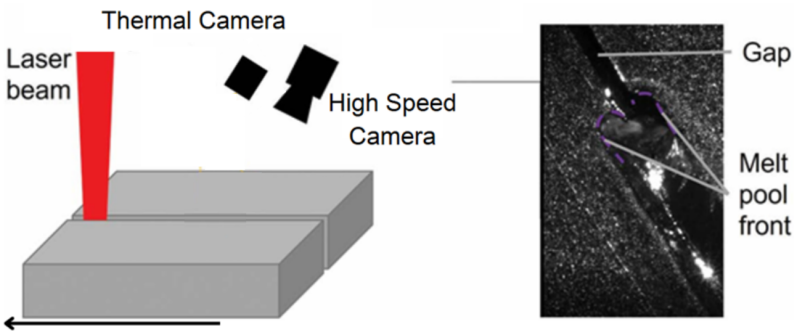

Figure 4.2
Camera System

4.2 Test preparation

To conduct butt welding experiments with controlled and repeatable gap tolerances, a simple custom fixture was developed, shows in Fig4.3. The fixture consists of a base plate, standardized clamps, and M8 positioning bolts, and is designed to accommodate two 50 mm × 100 mm stain-

less steel plates for welding. The base plate is mounted onto the conveyor system and aligned with the existing fixture interface (as shown in Figure 4.4) using central alignment holes and bolts.

To avoid heat-induced deformation or thermal influence on the alignment holes during welding, the weld seam is intentionally offset from the conveyor's central axis. M8 bolts serve as mechanical stops to ensure consistent joint configuration, while the standardized clamps are used to securely hold the plates in place throughout the welding process, providing stable conditions during testing.

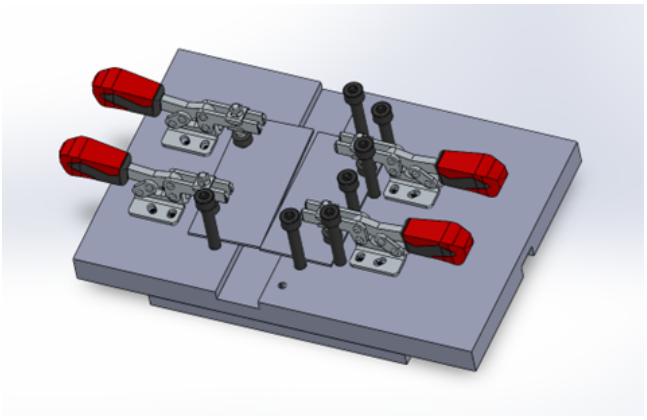

Figure 4.3
Fixture design

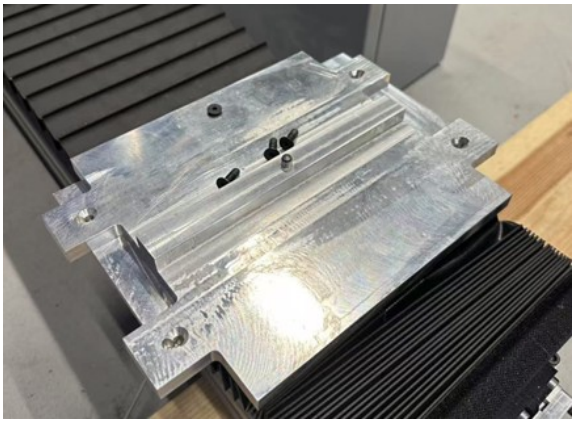

Figure 4.4
Conveyor mounting

Additionally, all 304 stainless steel specimens were prepared by cutting them into a uniform size of 50 mm × 100 mm for consistency across tests.

4.3 Test setup

Welding equipment set-up

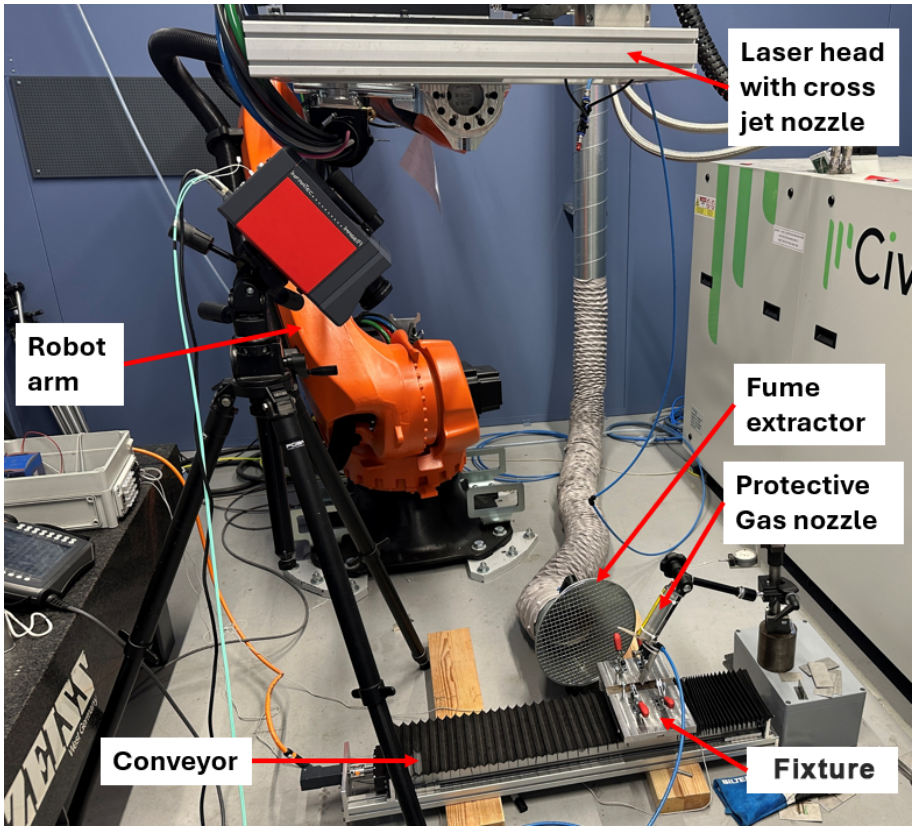

Figure 4.5
Welding setup

The experimental setup at the AAU Laser Laboratory is illustrated in Figure 4.5. At the core of the system is a high-power Optical Phased Array (OPA) laser provided by Civan, capable of delivering up to 14 kW output power. The laser source is a fiber laser operating at a wavelength of 1064 nm, with a beam quality factor of $M^2 = 1.2$. The system comprises 32 coherently combined fundamental-mode beams. A focal length of 1500 mm was selected for the experiments.

The OPA laser head is mounted on a KUKA robotic arm, which provides adjustability for focus position and welding area. The main laser unit is stationed to the right of the welding cell, and the shaped beam is delivered to the laser head via a fiber-optic cable suspended overhead. During welding, both the laser head and the robot remain stationary.

A horizontal conveyor belt is installed beneath the laser head to move the workpiece at controlled welding speeds, which can be set between 0 and 100 mm/s via synchronized programming with the laser. Custom-designed fixtures are mounted on the conveyor belt to securely hold the workpieces in place and to allow control over joint geometry.

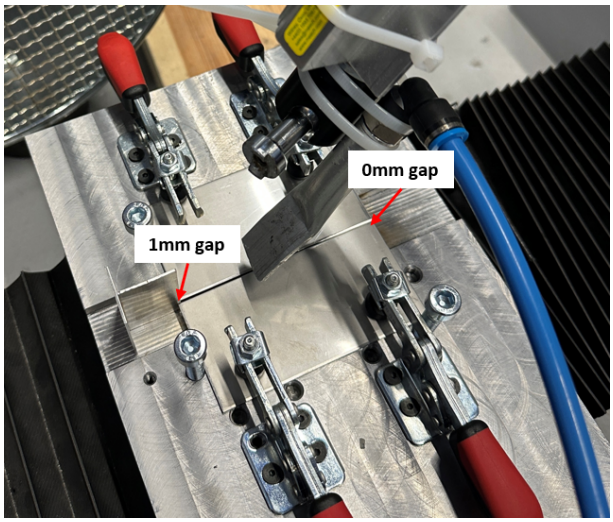

Figure 4.6
Workpieces in fixture

As shown in Figure 4.6, the test specimens consist of two AISI 304 stainless steel plates. The composition of 304 stainless steel shows in table 4.2. each 2 mm thick and measuring 100 mm by 50 mm. The plates are manually loaded and clamped into the fixture with certain joint geometry before welding. To account for the influence of shielding gas on melt pool behavior and potential gap bridging, a protective gas nozzle is positioned approximately 20 mm from the weld zone, aligned with the welding direction at an inclination angle of 60°.

In addition, a tripod fixture is installed diagonally above the setup to accommodate future installation of a thermal imaging camera or high-speed camera for process monitoring and analysis.

Table 4.2
Chemical composition of 304 stainless steel (weight %)

Element	**Minimum (%)**	**Maximum (%)**	**Typical (%)**
Carbon (C)	–	0.08	0.03–0.06
Manganese (Mn)	–	2.00	∼1.00
Phosphorus (P)	–	0.045	∼0.03
Sulfur (S)	–	0.030	∼0.01
Silicon (Si)	–	1.00	∼0.40
Chromium (Cr)	18.0	20.0	18.0–19.0
Nickel (Ni)	8.0	10.5	8.0–10.0
Nitrogen (N)	–	0.10	∼0.05
Iron (Fe)		Balance	

Beam pattern set-up

A total of 12 static beam patterns were designed and categorized based on their energy distribution continuity: **multi-spot patterns (Shapes 1–4)**, **multi-line patterns (Shapes 5–8 12)**, and **special continuous patterns (Shapes 9–11)**.

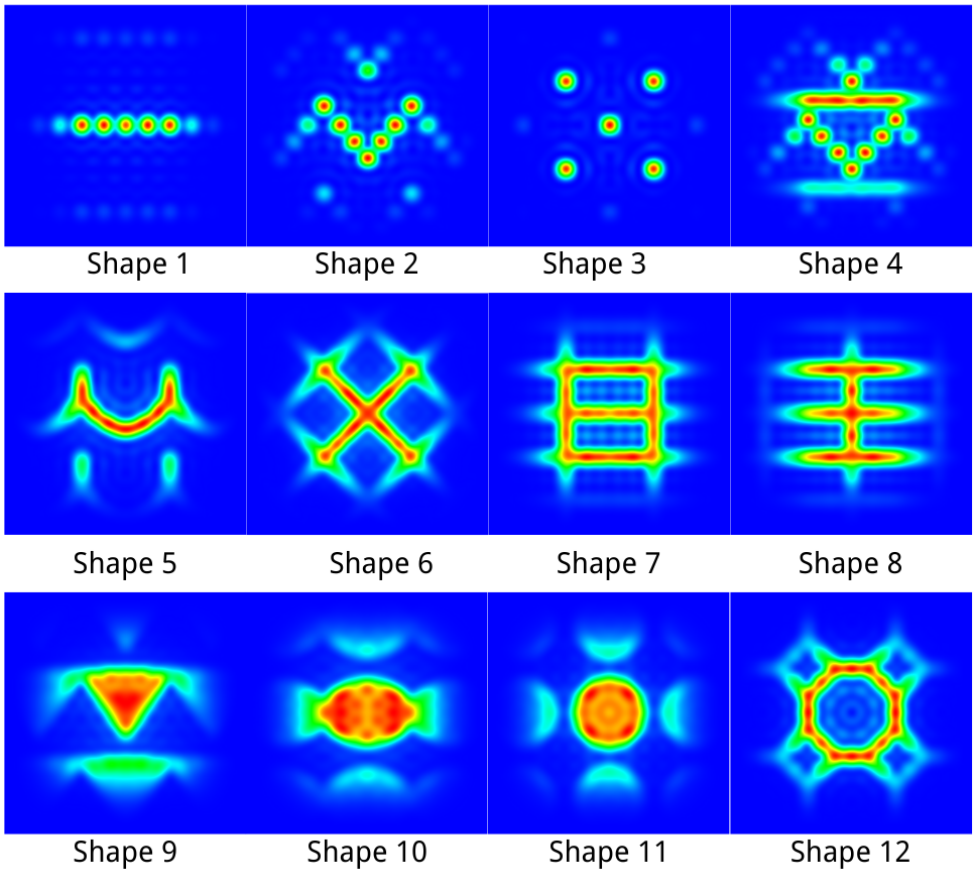

Figure 4.7
Designed Beam Shapes

Shapes 1–3: Multi-spot patterns

Shapes 1 to 3 are inspired by previous work on multiple-spot welding using diffractive optical elements (DOE), as demonstrated by Morten et al[35]. These patterns aim to investigate the fundamental mechanisms of multiple-spot welding with Civan's beam-shaping laser, particularly the influence of individual beamlets on melt pool behavior. In Shape 2, V-shaped configurations are employed to guide molten metal toward the joint center, thus enhancing gap-bridging performance. Shape 3 serves as a baseline pattern for purely mechanistic observation.

Shapes 4–8 12: Multi-line patterns

Shape 4 is preheated V-shaped and modified from shape 2, the continuity is higher than shape 2. Shapes 5 to 8 feature more continuous energy distribution compared to the first group. Shape 5 and Shape 6 are designed to examine the effect of increased continuity by comparing them directly with Shapes 1–4. Shapes 7 and 8 provide enhanced lateral energy input to generate wider melt pools and prolong their existence, supporting effective metal flow toward the gap. Shape 12 represents a common industrial profile—*O-ring*—and are included to compare custom patterns against widely used shapes.

Shapes 9–11: Special continuous patterns

Shapes 9 to 11 are unique continuous patterns with distinctive profiles. Shape 9, the continuous version of the V-shape, allows a direct comparison with its segmented counterpart to further assess the role of continuity. Shape 10 is a custom-designed, candy-like pattern intended to create an ultra-wide melt pool. Shapes 11 represent another common industrial profile—*top-hat* which are included to benchmark the custom patterns against widely used shapes.

All beam patterns were designed with a consistent width of approximately 700 μm, which corresponds to the maximum achievable beam width using the Civan dynamic beam-shaping laser.

Welding parameter set-up

Based on preliminary experiments conducted with a Gaussian beam on butt joints without gaps, it was observed that a laser power of 2500 W and a welding speed of 50 mm/s produced a stable keyhole and high-quality welds. Therefore, this parameter set was selected as a baseline and is referred to as **Condition 1**.

To simulate the potential reduction in power density caused by beam shaping—while maintaining a similar penetration depth—**Condition 2** was designed by increasing the power to 4500 W while keeping the speed constant at 50 mm/s.

Furthermore, to investigate the influence of welding speed on bridging performance, **Condition 3** was introduced by lowering the speed to 25 mm/s at the same power level of 2500 W. This condition reflects concerns that excessively high speeds may increase thermal gradients and cooling rates, thereby reducing the ability of the molten pool to bridge gaps.

Table 4.3

Welding parameters used in the gap bridging experiments

Condition	Laser Power (W)	Welding Speed (mm/s)	Purpose
Condition 1	2500	50	Baseline (Gaussian beam, produces stable keyhole and high-quality weld)
Condition 2	4500	50	Simulates reduced power density due to beam shaping, while maintaining penetration depth
Condition 3	2500	25	Evaluates effect of slower welding speed on thermal gradients and gap bridging behavior

Together, these three parameter sets allow a systematic evaluation of beam shaping effects under different energy inputs and welding speeds, enabling pairwise comparisons to assess gap bridging performance under varying thermal conditions.

In addition, nitrogen was used as the shielding gas, and the flow rate was uniformly set to 25L/min to eliminate the impact of the shielding gas on the molten pool.

Results analysis setup

Following the completion of the welding experiments, the analysis phase was carried out as illustrated in Figure 4.9. The maximum successful welding gap width and the presence of incompletely filled grooves were chosen as the primary evaluation indicators in the initial assessment, as shown in Figure 4.8.

The *maximum successful welding gap width* is defined as the gap width at the position where the weld terminates, indicating the largest gap that can be successfully bridged. In addition, according to the ISO 13919-1 standard [7, 47], imperfection No. 511—*Incompletely filled groove*—was also selected a evaluation criterion. This value reflects the extent of incomplete groove filling after welding and serves as a measure of the beam's gap-bridging capability.

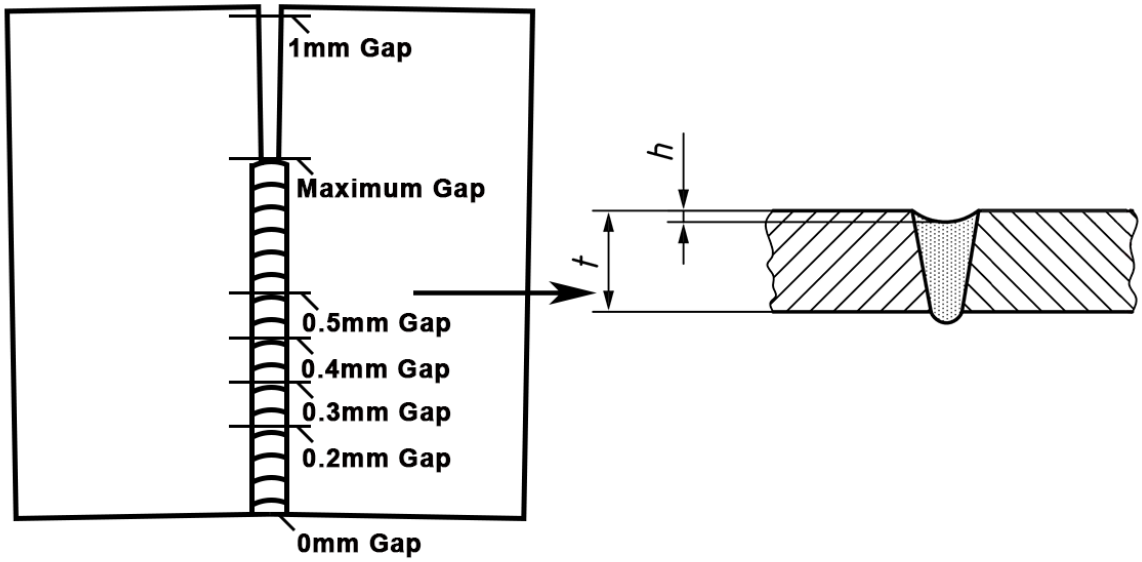

Figure 4.8
Maximum gap and incompletely filled groove according to ISO 13919-1 [47]

The first step involved identifying and quantifying the maximum gap width that each beam pattern could successfully bridge under different welding conditions. This was accomplished through a combination of visual inspection and physical measurement of the effective weld length.

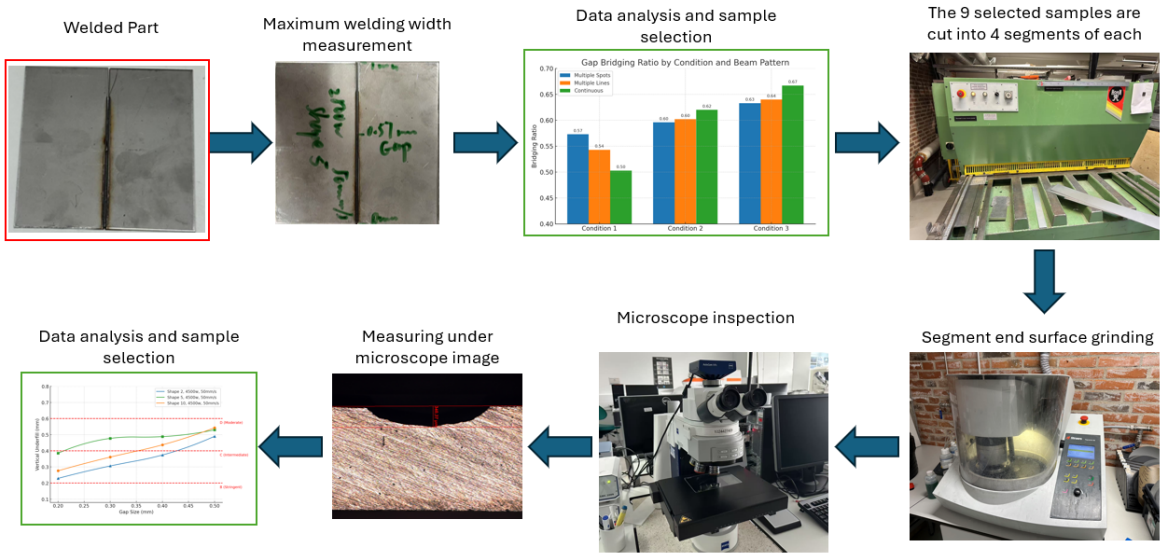

Figure 4.9
Analysis workflow

To calculate the maximum bridged gap width ($W_{\max}$), the following formula was applied:

$$W_{\max} = \left(\frac{100 \text{ mm} - 2 \text{ mm}}{1 \text{ mm}} \right) \times L_{\text{weld}}$$

where 100 mm is the total sample length, 2 mm accounts for the space occupied by the inserted plates, and 1 mm corresponds to the plate thickness, which also defines the designed maximum joint width. L_{weld} denotes the measured weld length.

After computing $W_{\max}$ for all samples, representative welds were selected for further microstructural analysis. A total of nine samples (one per beam pattern per condition) were chosen. Each sample was sectioned at four locations corresponding to nominal gap widths of 0.2 mm, 0.3 mm, 0.4 mm, and 0.5 mm.

The cross-sections were then ground and polished until the joint geometry became clearly visible. Microscopic inspection was performed, and the vertical distance from the lowest point of the fusion zone to the top surface was measured using high-resolution imaging. This measurement served as a quantitative indicator of the melt pool's gap-filling capability.

Finally, the collected data were analyzed to assess and compare the bridging performance of each beam pattern under varying welding conditions.

4.4 Results and discussion

This chapter presents and analyzes the experimental results, aiming to identify the influence of different beam shapes on gap bridging performance.

Figure 4.10 shows the average maximum gap width achieved by three beam shape categories under three welding conditions. These conditions are categorized as: (1) high speed and low power, (2) high speed and high power, and (3) low speed and low power.

Under Condition 1, the beam with the lowest continuity—Multiple Spots—exhibited the best bridging capability. As the spatial continuity of the beam increased, the bridging performance decreased. When the laser power was significantly increased (Condition 2), all beam types demonstrated improved performance. However, the improvement was most notable for the fully continuous pattern, while the Multiple Spots group only showed marginal gains. In Condition 3, where the speed was reduced but the power remained low, all beam types experienced a modest performance increase, likely due to reduced thermal gradients and longer melt pool lifetimes. These observations suggest that bridging capability is highly sensitive to both beam shape and thermal dynamics, warranting further investigation.

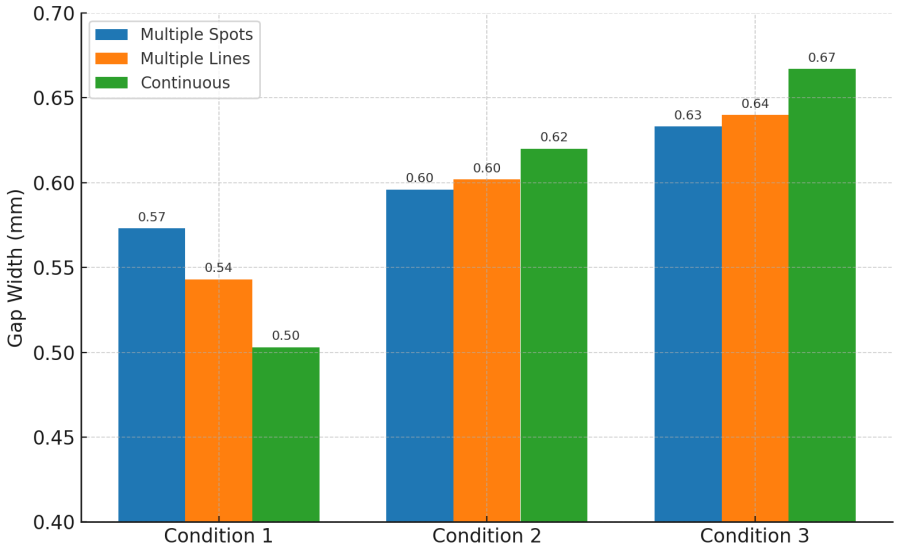

Figure 4.10

Average maximum bridged gap width for different beam shape groups under three welding conditions.

To better understand the bridging mechanism, one representative beam shape was selected from each category for further analysis—Shape 2 (Multiple Spots), Shape 5 (Multiple Lines), and Shape 10 (Continuous). As shown in Figure 4.11, Shape 2's performance closely approximates the group average for Multiple Spots, validating its representativeness. Shape 5 shares structural similarity with Shape 2 but features greater spatial continuity, making it valuable for comparative analysis. Shape 10, with its fully continuous pattern, initially performs poorly under low power conditions but shows dramatic improvement under high power, highlighting the thermal sensitivity of such beam shapes.

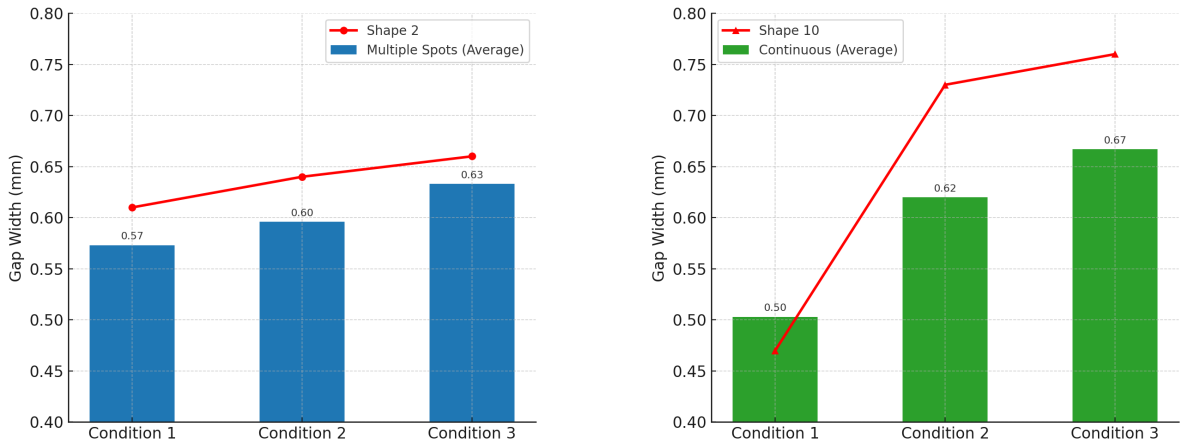

(a) Shape 2 in Multiple Spots group

(b) Shape 10 in Continuous group

Figure 4.11

Performance of representative beam shapes compared to their respective group averages.

According to the ISO 13919-1 standard [47], weld quality can be categorized into three classes—B (stringent), C (intermediate), and D (moderate)—based on the height (h) of the imperfection relative to the main plate thickness, as schematically illustrated in Figure 4.12. In this study, the h value is also adopted as a quantitative indicator of melt pool filling capability, and hence of gap bridging performance. A lower h value corresponds to better filling and stronger bridging capacity.

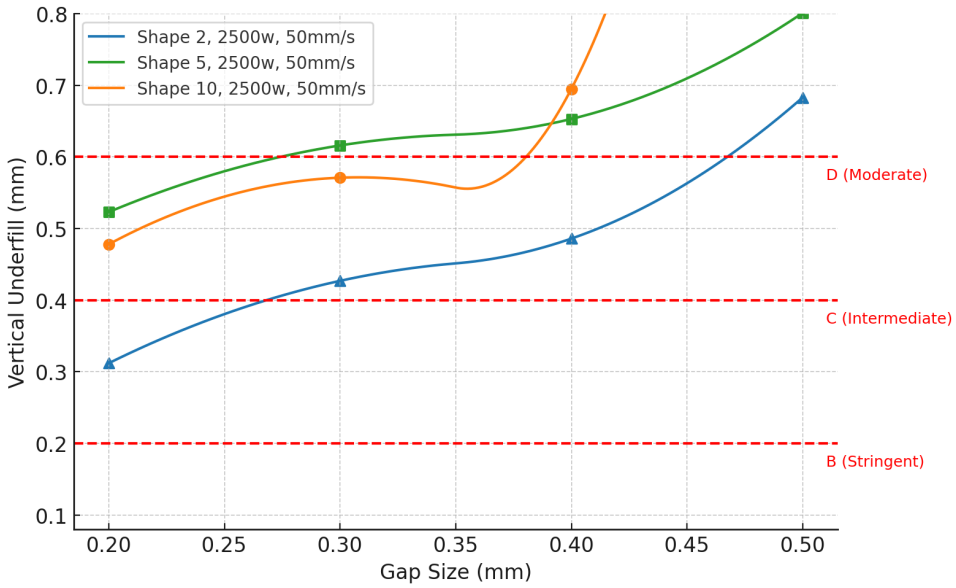

Figure 4.12

Measured h values versus gap width for different beam shapes under Condition 1 (high-speed, low-power).

As shown in Figure 4.12, under high-speed, low-power welding (Condition 1), Shape 2 demonstrates superior gap bridging across all tested gap widths, maintaining acceptable weld quality even at a 0.47 mm gap. Shape 10 performs slightly better than Shape 5 at narrower gaps (0.3 mm), but its performance rapidly degrades as the gap increases, eventually leading to bridging failure. Shape 5 consistently shows the poorest weld quality, and its deterioration trend

resembles that of Shape 2, albeit at a lower baseline.

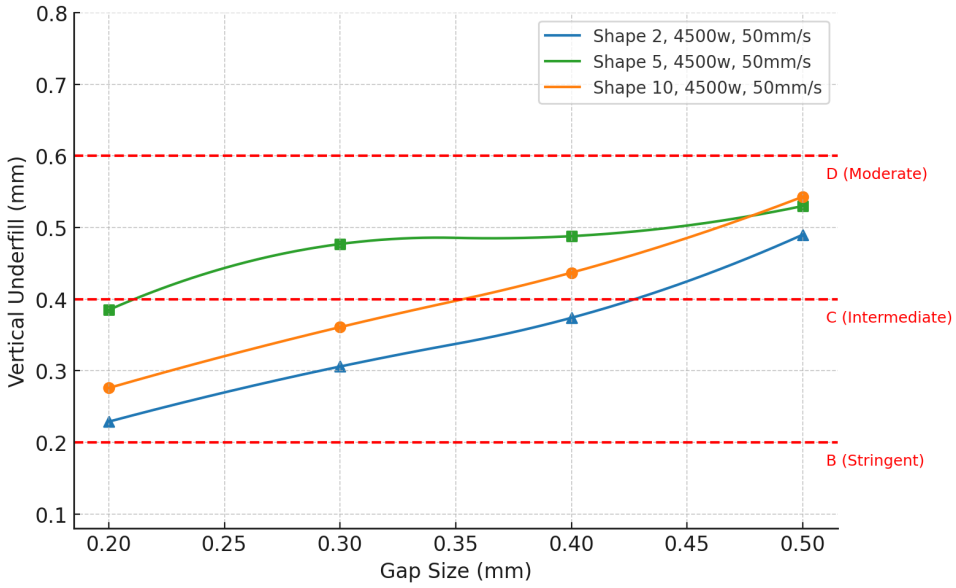

Figure 4.13
Measured h values versus gap width for different beam shapes under Condition 2 (high-speed, high-power).

Under Condition 2 (high-speed and high-power), all three beam shapes exhibit significant improvements in bridging performance, as shown in Figure 4.13. Among them, Shape 10 benefits the most from the increased power. This can be attributed to the nature of highly continuous beam shapes, which tend to have a lower peak power density due to energy spread, thus making it more difficult to establish a stable keyhole or melt pool under low-power conditions. When power is increased to 4500 W, Shape 10 achieves more effective keyhole formation, resulting in a dramatic improvement in bridging behavior.

This trend was also preliminarily observed in Figure 4.11, but requires further validation via metallographic cross-sectional analysis or in-situ high-speed imaging to confirm the welding mode (keyhole vs conduction).

Although Shape 5 shows reasonable h values under this condition, its overall bridging performance is still limited—the maximum bridged gap was only 0.57 mm, lower than Shape 10 (0.73 mm) and Shape 2 (0.64 mm). Figure 4.14 shows the weld surface of Shape 5 under Condition 2. A visible gap appears at the termination point, followed by an abrupt transition into molten material flow attempting to bridge the joint. This may be caused by premature solidification during the bridging process due to a high thermal gradient and insufficient energy deposition at the beam center in Shape 5, especially at high welding speeds.

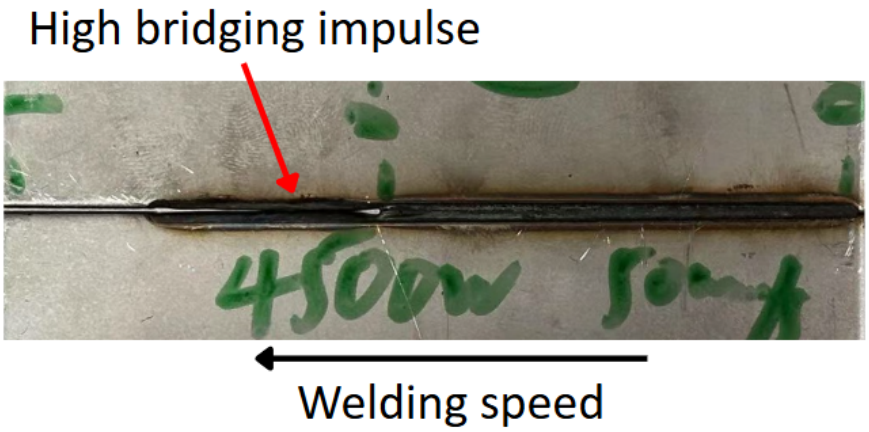

Figure 4.14
Weld surface of Shape 5 under Condition 2, showing incomplete bridging followed by melt redistribution.

Under the low-speed, low-power condition, the bridging behavior of the beam shapes changed significantly. The two beam patterns with higher spatial continuity exhibited considerable improvement in bridging performance, further supporting earlier observations. In contrast, the discontinuous Shape 2 showed a decline in performance—particularly at smaller gap widths—compared to its behavior under the high-speed, low-power setting.

Moreover, the degradation trend in bridging performance with increasing gap width was notably mitigated across all beam shapes. Shape 2 maintained a relatively stable height difference around 0.4–0.5 mm, suggesting altered melt pool dynamics. This could be attributed to reduced melt pool velocities at lower welding speeds, which may lead to partial beam transmission through the keyhole and suboptimal energy utilization. As a result, the molten material may lack sufficient driving force to refill the gap, while the surface melt may lose mobility due to insufficient thermal input

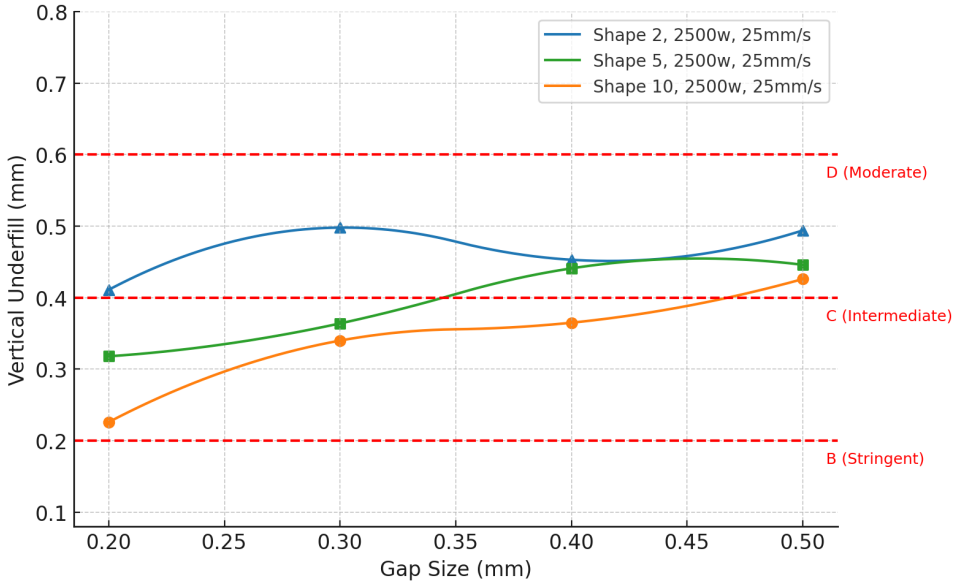

Figure 4.15
Measured h values versus gap width for different beam shapes under Condition 3 (Low-speed, Low-power)

At a fixed level of spatial continuity, the geometric arrangement of beam sub-patterns also plays a crucial role in gap bridging performance. As shown in Fig. 4.16, three different spatial arrangements of the multiple-spot pattern yield distinctly different outcomes. The simple linear pattern (Shape 1) consistently delivered the poorest performance under all welding conditions. In contrast, the V-shaped pattern in Shape 2 likely facilitated inward flow of the molten material, enhancing performance during high-speed welding. Shape 3, which concentrated energy at the beam edges, appears to have promoted sustained melt pools on both sides, enabling superior performance under low-speed, low-power conditions.

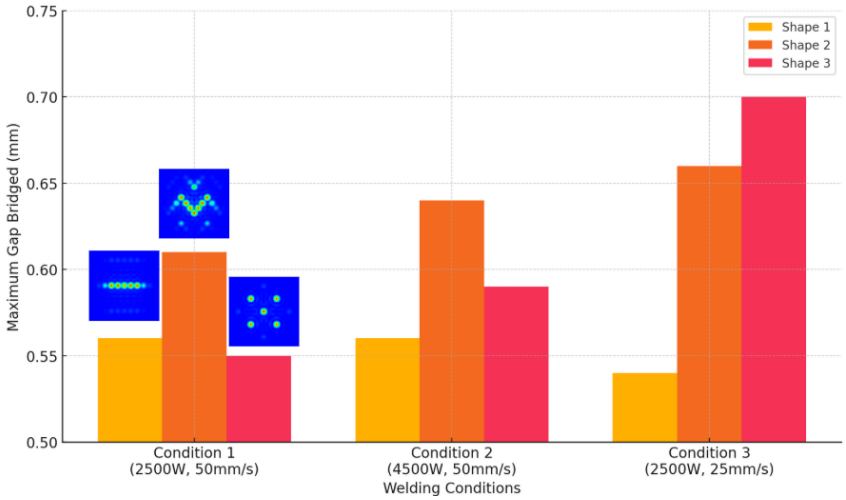

Figure 4.16
Gap bridging performance of shape 1,2,3 under different condition

4.5 Conclusion

In this study, 12 static beam patterns were evaluated under three different welding parameter sets. These patterns were categorized into three groups based on their spatial continuity. Gap bridging performance and weld quality were assessed using two key metrics: the maximum bridged gap width and the height difference defined by ISO 13919-1 standards. Based on the experimental results and subsequent analysis, the following conclusions can be drawn:

- Beam continuity has a substantial impact on peak laser intensity and, consequently, on gap bridging performance under the same welding parameters.
- Welding parameters significantly influence bridging behavior. In general, higher laser power and lower welding speed contribute to improved gap bridging due to increased energy input and reduced thermal gradients.
- Under high-speed, low-power conditions, discontinuous beam shapes such as Multiple Spots deliver superior bridging, likely due to their ability to form relatively stable keyholes despite lower power density.
- In contrast, under low-speed, low-power conditions, continuous beam profiles outperform others, likely because of their more uniform heat distribution, which sustains melt pool fluidity for longer durations.

- The spatial arrangement of sub-beams within a pattern also plays a critical role. V-shaped or edge-focused spot distributions are more effective in directing melt flow compared to linear arrangements, particularly under high-speed conditions. These effects appear to be driven by the interaction between beam intensity distribution and melt pool hydrodynamics.

Although several trends and mechanisms have been identified, further investigation—particularly using in-situ process diagnostics or advanced numerical simulations—is necessary to fully understand the underlying physical principles governing gap bridging in laser welding.

Solution proposal 5

To address the central question raised in Chapter 1 — *how can the gap bridging capability in laser butt welding be improved?* — this chapter presents a structured solution based on the conceptual framework introduced in Section 2.5.

The proposed solution involves the use of Optical Phased Arrays (OPA) and Coherent Beam Combining (CBC)-based beam shaping technologies to develop suitable beam patterns for specific welding tasks. These optimized patterns are then used to guide the design and manufacturing of Diffractive Optical Elements (DOE), which are integrated into the existing laser systems. By inserting the DOE into the collimated beam path, the system is upgraded to achieve enhanced gap bridging performance under industrial production conditions.

The overall workflow is illustrated in Figure 5.1 and can be divided into the following steps:

Step 1: Feasibility assessment of the solution

Upon receiving production line modification requests, the first step is to evaluate the feasibility of implementing the proposed solution on the existing system. The most critical factor is whether the current laser source supports DOE-based beam shaping. DOE technology, which manipulates wavefronts based on diffraction principles, is generally incompatible with broadband, multimode, high-power, or frequently wavelength-switched lasers. In addition, mechanical constraints such as limited space within the laser head may require significant redesign efforts, raising cost and complexity. Furthermore, the desired gap bridging performance must be compared against the solution's technical limits. If feasibility is deemed low, the process is terminated. Otherwise, the project proceeds to the next step.

Step 2: Welding process analysis

In this step, a detailed analysis of the existing welding process is conducted. This includes joint configuration analysis for relevant products, evaluation of welding cycle time, and target quality metrics. These data points are then used to configure a representative test platform and define optimization goals for beam shaping.

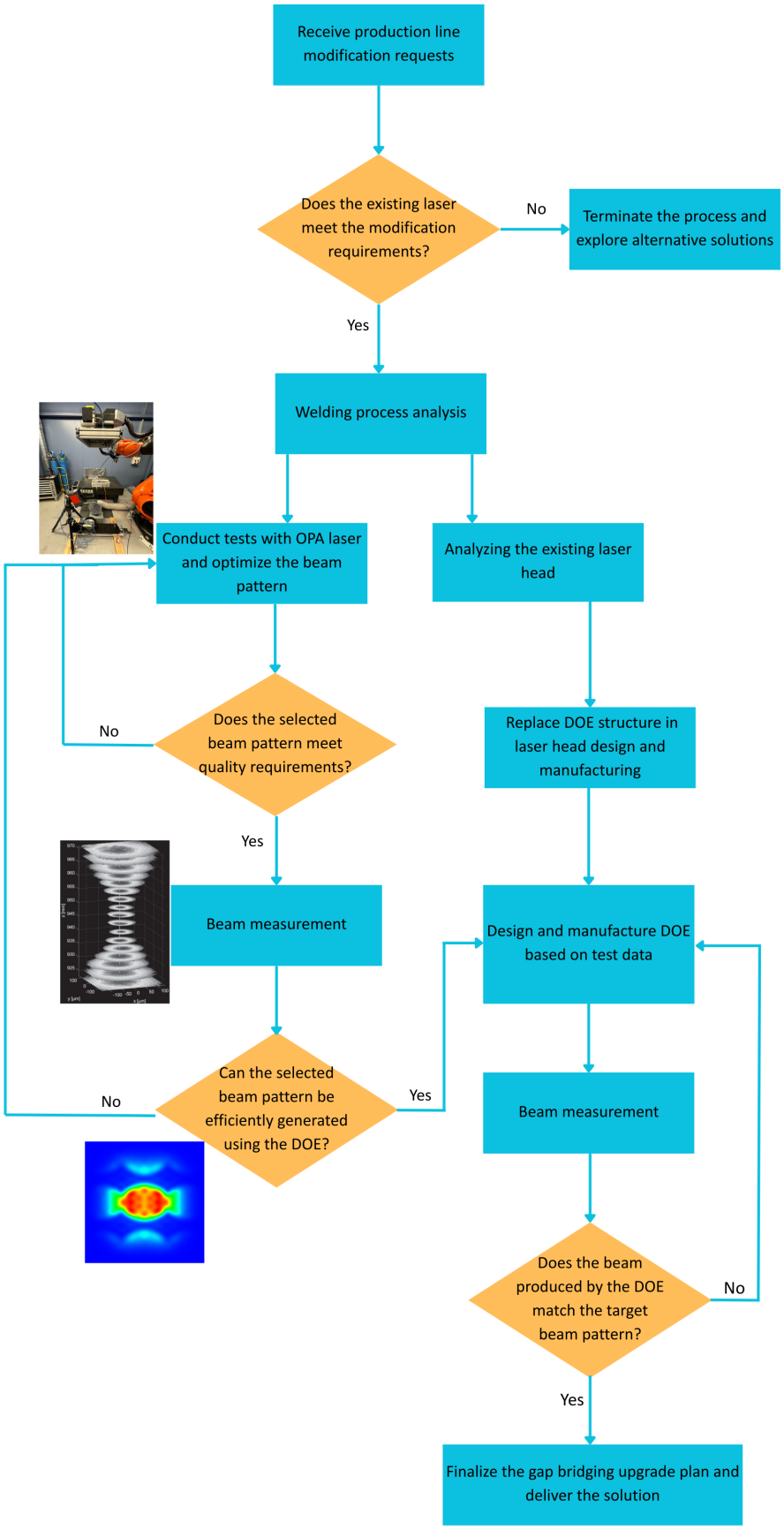

Figure 5.1
Solution for Improving Gap Bridging Capability in Existing Laser Welding Lines

Step 3: Experimental testing and laser head analysis

With process data collected, a test platform is set up in the OPA/CBC beam shaping laboratory. Beam patterns are designed based on theory and prior experience and tested under realistic conditions. The beam pattern that best meets the quality requirements is selected. Simultaneously, the existing laser head structure is analyzed to identify suitable integration points for the DOE.

Step 4: Beam measurement and DOE-compatible structure design

The selected beam pattern is evaluated through welding trials. If it fails to meet quality requirements, Step 3 is repeated with a new pattern. If successful, the beam is quantitatively measured using precision tools, such as the custom measurement box shown in Figure 5.2, which was developed as part of the author's VT-3 project.

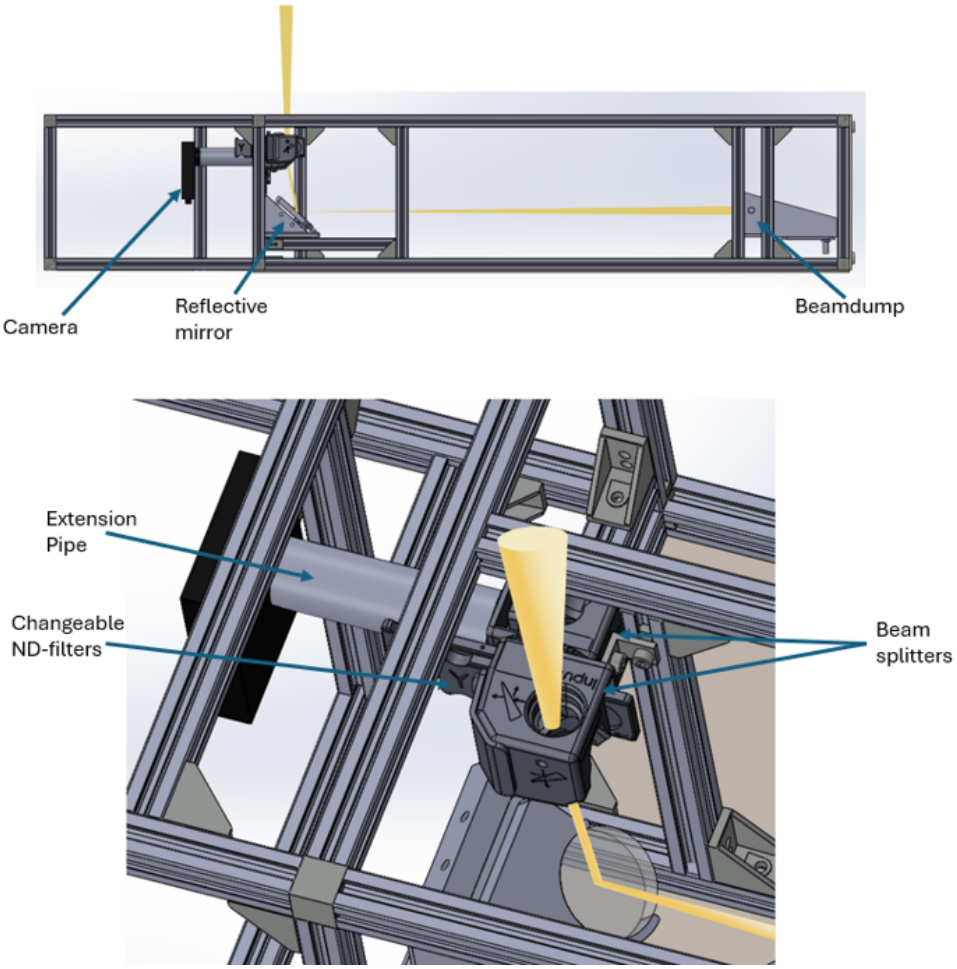

Figure 5.2
CAD model of the custom-built beam measurement box

Step 5: Feasibility evaluation of DOE generation and manufacturing

Based on the beam measurement data and target welding parameters, the feasibility of generating the selected pattern using a DOE is evaluated. Certain patterns may result in low efficiency or thermal deformation under high power or long-duration exposure. If feasibility is low, the process loops back to Step 3. If feasible, DOE design and manufacturing can begin, typically in collaboration with a specialized supplier.

Step 6: Validation of DOE-based beam shaping

Once the DOE is manufactured, it is validated under actual laser operating conditions using the same measurement box. The DOE-modified beam is compared to the previously tested pattern. If the match is confirmed, the system is assembled and final welding tests are performed. The complete bridging enhancement package is then delivered for industrial implementation.

Conclusion 6

This project began with a fundamental question identified in earlier research:

> *How can the gap bridging capability in laser butt welding be improved?*

To address this question, the physical principles of gap bridging in laser welding were first reviewed, along with an overview of existing techniques aimed at improving this capability. Among the various strategies, beam shaping emerged as a promising and experimentally validated method for controlling the shape and dynamics of the melt pool. However, current research primarily focuses on comparing different beam shaping techniques, without providing a systematic study of how specific beam profiles influence gap bridging. Moreover, many existing solutions face challenges in terms of cost, flexibility, and industrial applicability.

To overcome these limitations, a conceptual solution was proposed in Chapter 2.5. This approach involves using Optical Phased Arrays (OPA) and Coherent Beam Combining (CBC) to experimentally develop optimized beam profiles. These profiles then serve as the basis for designing and manufacturing Diffractive Optical Elements (DOE), enabling cost-effective implementation of static beam shaping in industrial production environments.

To explore this concept, a series of experiments were conducted at the AAU Flexible Laser Lab using a CIVAN dynamic laser. These experiments aimed to address the core scientific question:

> *How do different laser beam profiles influence gap bridging capability in autogenous butt welding, and what physical mechanisms underlie their effectiveness?*

Our findings suggest that quasi-static beam shaping can effectively enhance gap bridging performance. Experimental data revealed how different beam profiles influence weld quality, providing practical insights for DOE-based beam shaping design. However, the underlying mechanisms—particularly the melt pool dynamics under different beam conditions—remain incompletely understood. Further experimental and numerical investigations are needed to clarify these physical interactions.

In conclusion, this study demonstrates that using dynamic lasers to develop optimized static beam profiles, followed by their implementation via DOE-based shaping systems, offers a promising path toward improving gap bridging capability in industrial laser welding. Nonetheless, fur-

ther research is required to fully understand the physical mechanisms involved and to refine the design process for broader industrial application.

Future Work 7

Based on the current progress of this project, future work can be divided into short-term and long-term tasks.

Short-term tasks

Several experimental tasks remain to be completed. One of the key next steps is to capture and analyze the dynamic behavior of the melt pool during gap bridging. This should be done using high-speed cameras and infrared thermal imaging. By observing the melt pool in real time, we can better understand the physical mechanisms by which different beam profiles influence bridging performance.

In addition to melt pool observation, further validation of the weld quality is necessary. Metallographic analysis should be carried out to determine whether the welding process under different beam conditions operates in keyhole or conduction mode. This is especially important in cases where laser power is limited, and it will help confirm the interpretations made in earlier experiments.

Post-weld inspection can also be enhanced. Techniques such as X-ray CT scanning can be used to evaluate internal porosity, while mechanical testing—such as tensile or shear tests—can be conducted to assess the structural performance of the welds. These additional tests will provide a more comprehensive evaluation of weld quality.

Long-term directions

For long-term development, the proposed solution should be further refined and adapted for industrial application. The first step involves investigating suitable DOE laser shaping technologies, including DOE shapers, diffusers, or splitters. The choice depends on the desired beam pattern and the application's specific requirements.

Based on the experimental data obtained so far, prototype DOE components can then be designed and manufactured. These components should be tested using compatible laser systems that operate within safe power ranges. In parallel, a technical route should be developed for integrating replaceable DOE structures into existing laser head assemblies.

Finally, comparative welding trials should be conducted. These experiments would use both dynamic and static lasers to apply the same beam pattern under identical welding parameters. The goal is to evaluate the performance difference between the two systems and to assess whether static DOE-based shaping can achieve similar or better results in a production environment.

Literature

[1] Liping Guo et al. "Quantifying the effects of gap on the molten pool and porosity formation in laser butt welding." In: *International Journal of Heat and Mass Transfer* 209 (2023), p. 124143. ISSN: 0017-9310. DOI: https://doi.org/10.1016/j.ijheatmasstransfer.2023.124143. URL: https://www.sciencedirect.com/science/article/pii/S001793102300296X.

[2] Dapeng Wang et al. "Determination of beam incidence conditions based on the analysis of laser interference patterns." In: *Optik* 126.21 (2015), pp. 2902–2907. ISSN: 0030-4026. DOI: https://doi.org/10.1016/j.ijleo.2015.07.039. URL: https://www.sciencedirect.com/science/article/pii/S0030402615005914.

[3] Joerg Volpp. *High-Power Laser Material Processing for Engineers*. Boca Raton, FL: CRC Press, 2021. ISBN: 978-0-367-36457-9.

[4] Lucintel. *Laser Welding Market: Trends, Opportunities and Competitive Analysis 2023-2028*. Accessed: 2024-12-17. 2023. URL: https://www.researchandmarkets.com/reports/5802255/laser-welding-market-trends-opportunities-and.

[5] Z Sun and M Kuo. "Bridging the joint gap with wire feed laser welding." In: *Journal of Materials Processing Technology* 87.1 (1999), pp. 213–222. ISSN: 0924-0136. DOI: https://doi.org/10.1016/S0924-0136(98)00346-X. URL: https://www.sciencedirect.com/science/article/pii/S092401369800346X.

[6] Morgan Nilsen et al. "Robust vision-based joint tracking for laser welding of curved closed-square-butt joints." In: *The International Journal of Advanced Manufacturing Technology* 101.5-8 (2019), pp. 1967–1978. DOI: 10.1007/s00170-018-3044-0.

[7] International Organization for Standardization. *ISO 9692-1:2013 Welding and allied processes – Recommendations for joint preparation – Part 1: Manual metal arc welding, gas-shielded metal arc welding, gas welding and beam welding*. https://www.iso.org/standard/54901.html. Accessed: 2025-05-06. 2013.

[8] Muhammad Waqas et al. "Experimental and statistical investigation of laser welding with different joint gap widths for HSLA steel." In: *Smart Materials in Manufacturing* 2 (2024), p. 100057. ISSN: 2772-8102. DOI: https://doi.org/10.1016/j.smmf.2024.100057. URL: https://www.sciencedirect.com/science/article/pii/S277281022400014X.

[9] Partha Saha and Dhanraj Waghmare. "Parametric optimization for autogenous butt laser welding of sub-millimeter thick SS 316 sheets using central composite design." In: *Optics Laser Technology* 122 (2020), p. 105833. ISSN: 0030-3992. DOI: https://doi.org/10.1016/j.optlastec.2019.105833. URL: https://www.sciencedirect.com/science/article/pii/S003039921930581X.

[10] Mikhail Sokolov et al. "Laser welding of structural steels: Influence of the edge roughness level." In: *Optics Laser Technology* 44.7 (2012), pp. 2064–2071. ISSN: 0030-3992. DOI: https://doi.org/10.1016/j.optlastec.2012.03.025. URL: https://www.sciencedirect.com/science/article/pii/S0030399212001351.

[11] Yongcui Mi et al. "Beam shaping with a deformable mirror for gap bridging in autogenous laser butt welding." In: *Optics and Lasers in Engineering* 169 (2023), p. 107724. ISSN: 0143-8166. DOI: https://doi.org/10.1016/j.optlaseng.2023.107724. URL: https://www.sciencedirect.com/science/article/pii/S0143816623002531.

[12] Theodore H Maiman. "Stimulated optical radiation in ruby." In: *nature* 187.4736 (1960), pp. 493–494.

[13] Alan E. Willner et al. "Optics and Photonics: Key Enabling Technologies." In: *Proceedings of the IEEE* 100.Special Centennial Issue (2012), pp. 1604–1643. DOI: 10.1109/JPROC.2012.2190174.

[14] Klaus Schutt Hansen. "Multispot fiber laser welding." PhD thesis. Aalborg University, 2015. URL: https://doi.org/10.5278/vbn.phd.engsci.00043.

[15] C. T. Dawes. *Laser Welding: Principles and Applications*. London: Springer, 1992. ISBN: 9780412362408.

[16] Alexander F. H. Kaplan. "Model of the absorption variation during pulsed laser heating applied to welding of electronic Au/Ni-coated Cu-leadframes." In: *Applied Surface Science* 241.3-4 (Mar. 2005), pp. 362–370. DOI: 10.1016/j.apsusc.2004.07.035.

[17] John Dowden and Wolfgang Schulz. *The Theory of Laser Materials Processing: Heat and Mass Transfer in Modern Technology*. Second Edition. Vol. 119. Springer Series in Materials Science. Springer, 2017. DOI: 10.1007/978-3-319-56711-2.

[18] *Safety of machinery – Laser processing machines – Part 1: General safety requirements*. Standard. Geneva, Switzerland: International Organization for Standardization, 2005.

[19] Peter Schaaf, ed. *Laser Processing of Materials: Fundamentals, Applications and Developments*. Vol. 139. Springer Series in Materials Science. Berlin, Heidelberg: Springer, 2010. ISBN: 978-3-642-13280-3. DOI: 10.1007/978-3-642-13281-0.

[20] S. Cui, P. Dai, R. Ma, et al. "Mechanism study of flow characteristics of molten pool and keyhole dynamic behavior of K-TIG welding." In: *International Journal of Advanced Manufacturing Technology* 130 (2024), pp. 1195–1206. DOI: 10.1007/s00170-023-12743-w.

[21] Shengyong Pang et al. "3D transient multiphase model for keyhole, vapor plume, and weld pool dynamics in laser welding including the ambient pressure effect." In: *Optics and Lasers in Engineering* 74 (2015), pp. 47–58. ISSN: 0143-8166. DOI: https://doi.org/10.1016/j.optlaseng.2015.05.003. URL: https://www.sciencedirect.com/science/article/pii/S0143816615001141.

[22] Carlo Giovanni FERRO, Sara VARETTI, and Paolo MAGGIORE. "Experimental evaluation of mechanical compression of lattice trusses made with Ti6Al4V for aerospace use." In: *Chinese Journal of Aeronautics* 37.5 (2024), pp. 520–532. ISSN: 1000-9361. DOI: https://doi.org/10.1016/j.cja.2024.02.005. URL: https://www.sciencedirect.com/science/article/pii/S1000936124000499.

[23] Jicheng Chen et al. "Metal bridging characteristics and button-hole suppression mechanisms in pulse waveform-integrated oscillation laser beam welding (OLBW) of Ti6Al4V sheets under an air gap condition: A hydrodynamic perspective." In: *Journal of Manufacturing Processes* 148 (2025), pp. 24–44. ISSN: 1526-6125. DOI: https://doi.org/10.1016/j.jmapro.2025.05.006. URL: https://www.sciencedirect.com/science/article/pii/S1526612525005341.

[24] Jicheng Chen et al. "Weld pool dynamics and joining mechanism in pulse wave laser beam welding of Ti-6Al-4V titanium alloy sheets assembled in butt joint with an air gap." In: *Optics and Laser Technology* 146 (2022), p. 107558. ISSN: 0030-3992. DOI: https://doi.org/10.1016/j.optlastec.2021.107558. URL: https://www.sciencedirect.com/science/article/pii/S0030399221006460.

[25] Jicheng Chen et al. "Effects of groove clearance size on gap bridging capacity in PWLBW of Ti6Al4V alloy sheet assembled in butt joint configuration: Numerical simulation and experimental assessment." In: *Optics Laser Technology* 156 (2022), p. 108527. ISSN: 0030-3992. DOI: https://doi.org/10.1016/j.optlastec.2022.108527. URL: https://www.sciencedirect.com/science/article/pii/S0030399222006788.

[26] Lei Shao et al. "A review on combustion behavior and mechanism of Ti alloys for advanced aero-engine." In: *Journal of Alloys and Compounds* 960 (2023), p. 170584. ISSN: 0925-8388. DOI: https://doi.org/10.1016/j.jallcom.2023.170584. URL: https://www.sciencedirect.com/science/article/pii/S092583882301887X.

[27] M. Dal and R. Fabbro. "[INVITED] An overview of the state of art in laser welding simulation." In: *Optics Laser Technology* 78 (2016). The year of light: optical fiber sensors and laser material processing, pp. 2–14. ISSN: 0030-3992. DOI: https://doi.org/10.1016/j.optlastec.2015.09.015. URL: https://www.sciencedirect.com/science/article/pii/S0030399215002595.

[28] Yuhang Duan et al. "Documenting weld pool behavior differences in variable-gap laser self-melting and wire-filling welding of titanium alloys." In: *International Journal of Thermal Sciences* 210 (2025), p. 109550. ISSN: 1290-0729. DOI: https://doi.org/10.1016/j.ijthermalsci.2024.109550. URL: https://www.sciencedirect.com/science/article/pii/S1290072924006720.

[29] Bernard Johan Aalderink, B. Pathiraj, and R.G.K.M. Aarts. "Seam gap bridging of laser based processes for the welding of aluminium sheets for industrial applications." In: *International Journal of Advanced Manufacturing Technology* 48.1-4 (2010). Cited by: 43, pp. 143–154. DOI: 10.1007/s00170-009-2270-x. URL: https://www.scopus.com/inward/record.uri?eid=2-s2.0-77954215579&doi=10.1007%2fs00170-009-2270-x&partnerID=40&md5=511271ca488982eaea70f1a77958ca8b.

[30] A. Salminen. "The filler wire - Laser beam interaction during laser welding with low alloyed steel filler wire." In: *Mechanika* 84.4 (2010). Cited by: 66, pp. 67–74. URL: https://www.scopus.com/inward/record.uri?eid=2-s2.0-78249273003&partnerID=40&md5=a2d0166d5d05a4b895ce5dc03e32f4f8.

[31] Hanxuan Huang et al. "Research on weld formation mechanism of laser-MIG arc hybrid welding with butt gap." In: *Optics Laser Technology* 133 (2021), p. 106530. ISSN: 0030-3992. DOI: https://doi.org/10.1016/j.optlastec.2020.106530. URL: https://www.sciencedirect.com/science/article/pii/S0030399220311634.

[32] Villads Schultz. "Process stability during laser beam welding with beam oscillation and wire feed." In: *Journal of Manufacturing and Materials Processing* 3.1 (2019). Cited by: 10; All Open Access, Gold Open Access, Green Open Access. DOI: 10.3390/jmmp3010017. URL: https://www.scopus.com/inward/record.uri?eid=2-s2.0-85079836157&doi=10.3390%2fjmmp3010017&partnerID=40&md5=cf4f165317139207cf2f27ac69dcaf4e.

[33] Peter Haglund et al. "Surface tension stabilized laser welding (donut laser welding)—A new laser welding technique." In: *Journal of Laser Applications* 25.3 (Mar. 2013), p. 031501. ISSN: 1042-346X. DOI: 10.2351/1.4798219. eprint: https://pubs.aip.org/lia/jla/article-pdf/doi/10.2351/1.4798219/13761007/031501_1_online.pdf. URL: https://doi.org/10.2351/1.4798219.

[34] J. Volpp. "Multispot laser welding for increased gap bridgability." In: *Journal of Laser Applications* 34 (Nov. 2022), p. 042002. DOI: 10.2351/7.0000724.

[35] Morten Kristiansen et al. "Single Pass Laser Welding with Multiple Spots to Join Four Sheets in a Butt-joint Configuration." In: *Physics Procedia* 89 (2017). 16th Nordic Laser Materials Processing Conference, NOLAMP16, pp. 205–213. ISSN: 1875-3892. DOI: https://doi.org/10.1016/j.phpro.2017.08.021. URL: https://www.sciencedirect.com/science/article/pii/S1875389217301475.

[36] Thomas Stoll et al. "Influence of laser beam shaping on the cracking behavior of tungsten at single weld lines." In: *International Journal of Refractory Metals and Hard Materials* 125 (2024), p. 106864. ISSN: 0263-4368. DOI: https://doi.org/10.1016/j.ijrmhm.2024.106864. URL: https://www.sciencedirect.com/science/article/pii/S0263436824003123.

[37] Klaus Hansen, Morten Kristiansen, and Flemming Olsen. "Beam Shaping to Control of Weldpool Size in Width and Depth." In: *Physics Procedia* 56 (Dec. 2014), pp. 467–476. DOI: 10.1016/j.phpro.2014.08.150.

[38] K. S. Hansen et al. "Joining of multiple sheets in a butt-joint configuration using single pass laser welding with multiple spots." In: *Journal of Laser Applications* 27.3 (2015), p. 032011. DOI: 10.2351/1.4922222.

[39] C. Prieto et al. "Dynamic laser beam shaping for laser aluminium welding in e-mobility applications." In: *Procedia CIRP* 94 (2020). 11th CIRP Conference on Photonic Technologies [LANE 2020], pp. 596–600. ISSN: 2212-8271. DOI: https://doi.org/10.1016/j.procir.2020.09.084. URL: https://www.sciencedirect.com/science/article/pii/S2212827120312695.

[40] D. Dittrich et al. "Laser beam welding of hot crack sensitive Al-alloys without filler wire by intensity controlled dynamic beam oscillation." In: *Procedia CIRP* 111 (2022). 12th CIRP Conference on Photonic Technologies [LANE 2022], pp. 435–438. ISSN: 2212-8271. DOI: https://doi.org/10.1016/j.procir.2022.08.182. URL: https://www.sciencedirect.com/science/article/pii/S2212827122010769.

[41] Davide Maria Boldrin et al. "Seam tracking and gap bridging during robotic laser beam welding via grayscale imaging and wobbling." In: *Robotics and Computer-Integrated Manufacturing* 89 (2024), p. 102774. ISSN: 0736-5845. DOI: https://doi.org/10.1016/j.rcim.2024.102774. URL: https://www.sciencedirect.com/science/article/pii/S0736584524000607.

[42] Jonas Sebastian Rinne et al. "Advantages of adjustable intensity profiles for laser beam welding of steel copper dissimilar joints." In: *Procedia CIRP* 94 (2020). 11th CIRP Conference on Photonic Technologies [LANE 2020], pp. 661–665. ISSN: 2212-8271. DOI: https://doi.org/10.1016/j.procir.2020.09.103. URL: https://www.sciencedirect.com/science/article/pii/S2212827120312907.

[43] Masoud Mohammadpour et al. "Adjustable ring mode and single beam fiber lasers: A performance comparison." In: *Manufacturing Letters* 25 (2020), pp. 50–55. ISSN: 2213-8463. DOI: https://doi.org/10.1016/j.mfglet.2020.07.003. URL: https://www.sciencedirect.com/science/article/pii/S2213846320301346.

[44] Civan Lasers. *Methodology for Utilizing Dynamic Beam Laser Parameters*. Customer Seminar Presentation. Slide presented at the Customer Seminar on September 11, 2024. Sept. 2024.

[45] Nina Armon et al. "Encountering humping-driven defects using dynamic beam lasers." In: *12th CIRP Conference on Photonic Technologies [LANE 2022]*. Civan Advanced Technologies LTD. Jerusalem, Israel, 2022.

[46] Wei Yin. *Beam Shaping Technology: Effects on Molten Pool Behavior and Welding Defects, and Design of a Beam Measurement Box.(Exploring the Application of Beam Shaping in Mass-production)*. eng. 2025.

[47] *Electron and laser-beam welded joints — Requirements and recommendations on quality levels for imperfections — Part 1: Steel, nickel, titanium and their alloys*. Standard. Geneva, Switzerland: International Organization for Standardization, 2019.

Appendix A

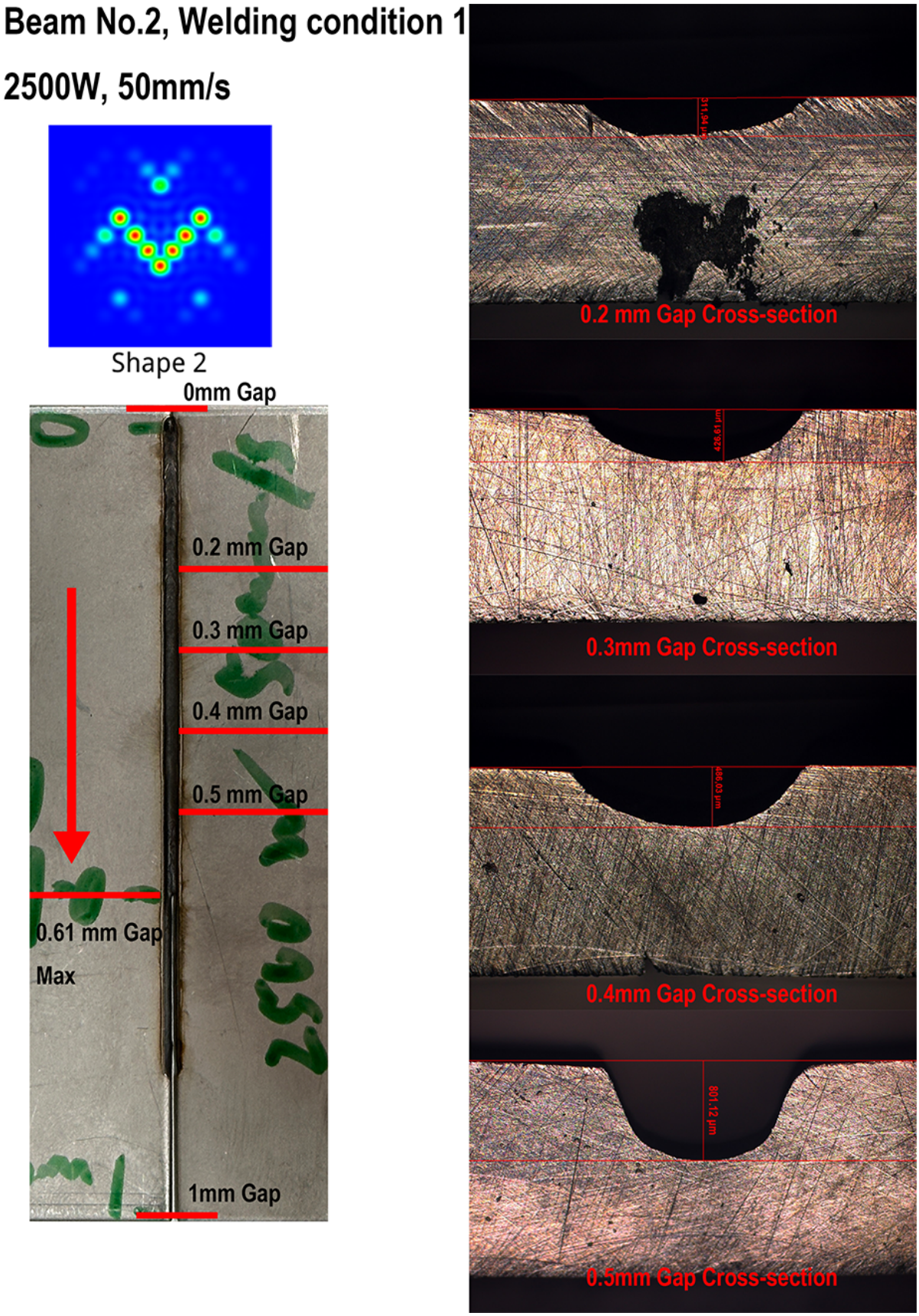

Figure A.1
Original Picture of shape 2 in welding condition 1

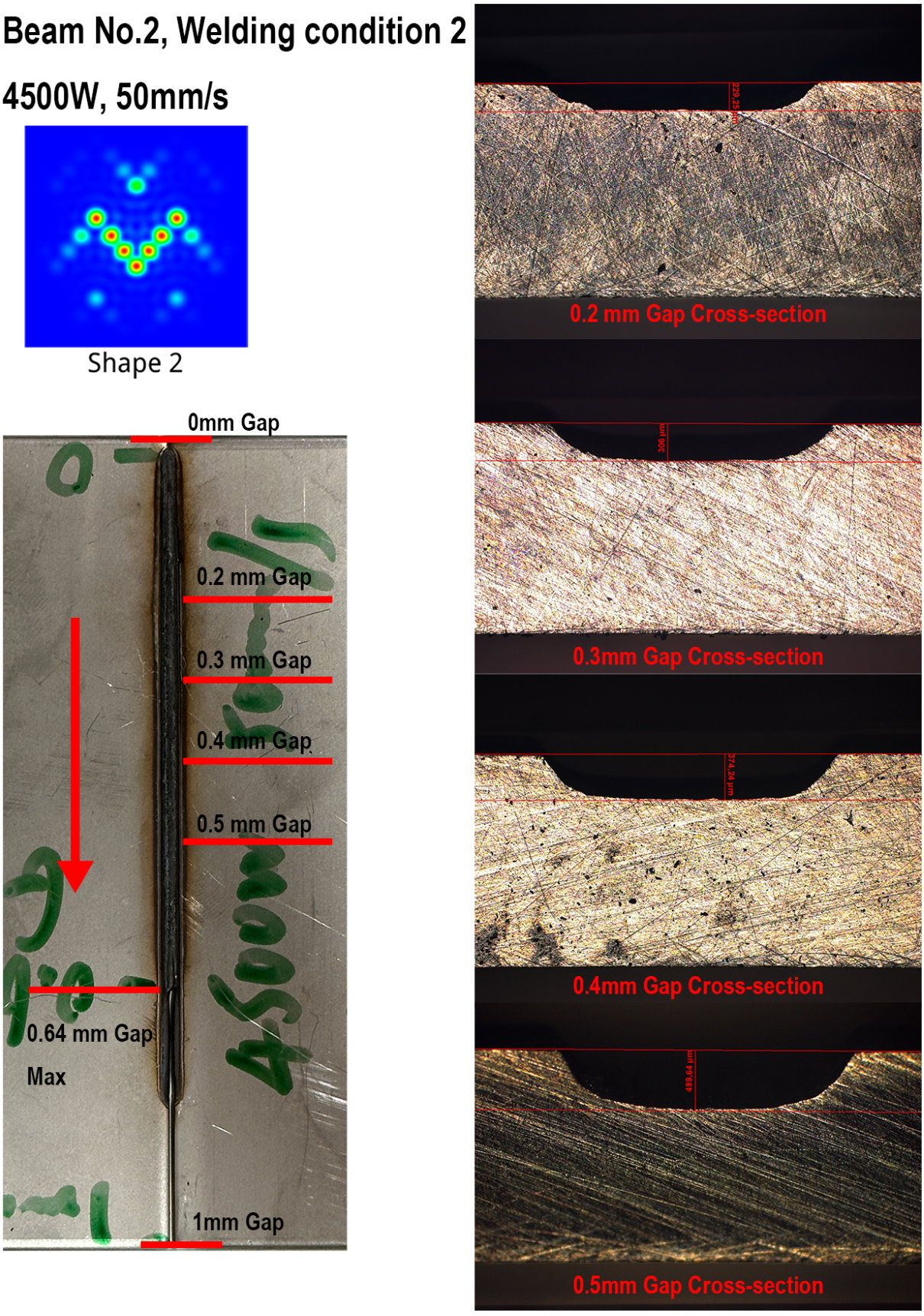

Figure A.2

Original Picture of shape 2 in welding condition 2

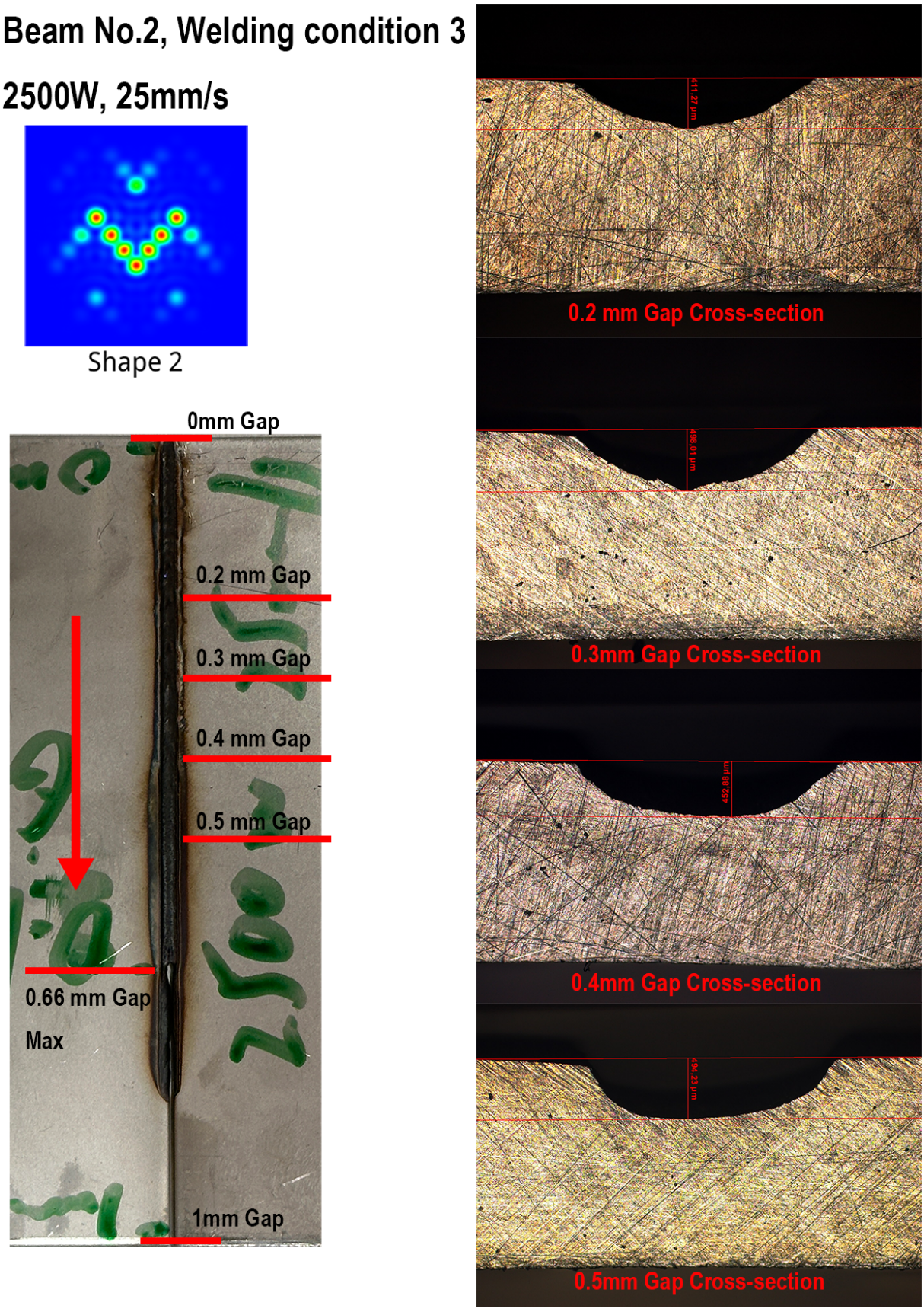

Figure A.3

Original Picture of shape 2 in welding condition 3

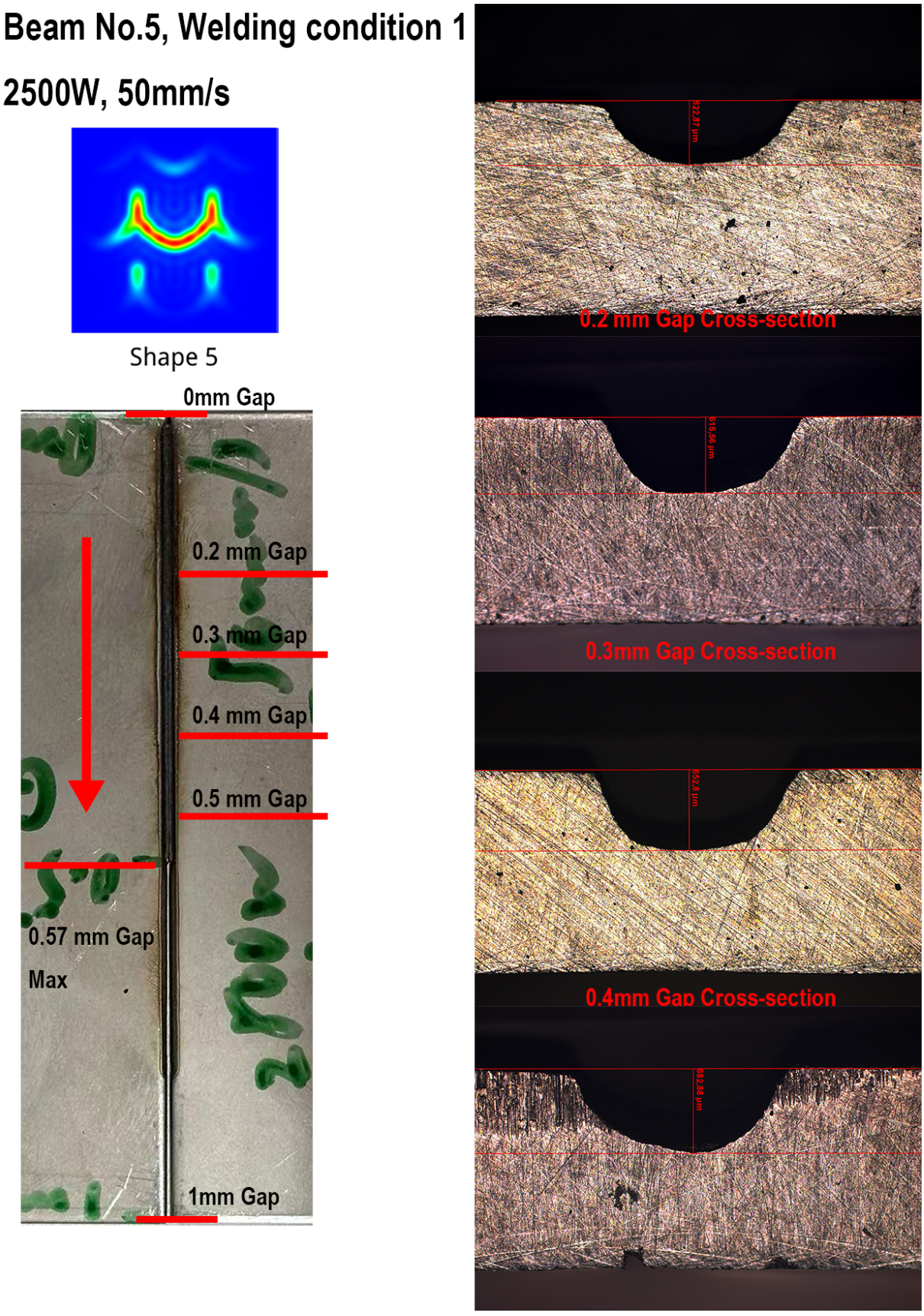

Figure A.4
Original Picture of shape 5 in welding condition 1

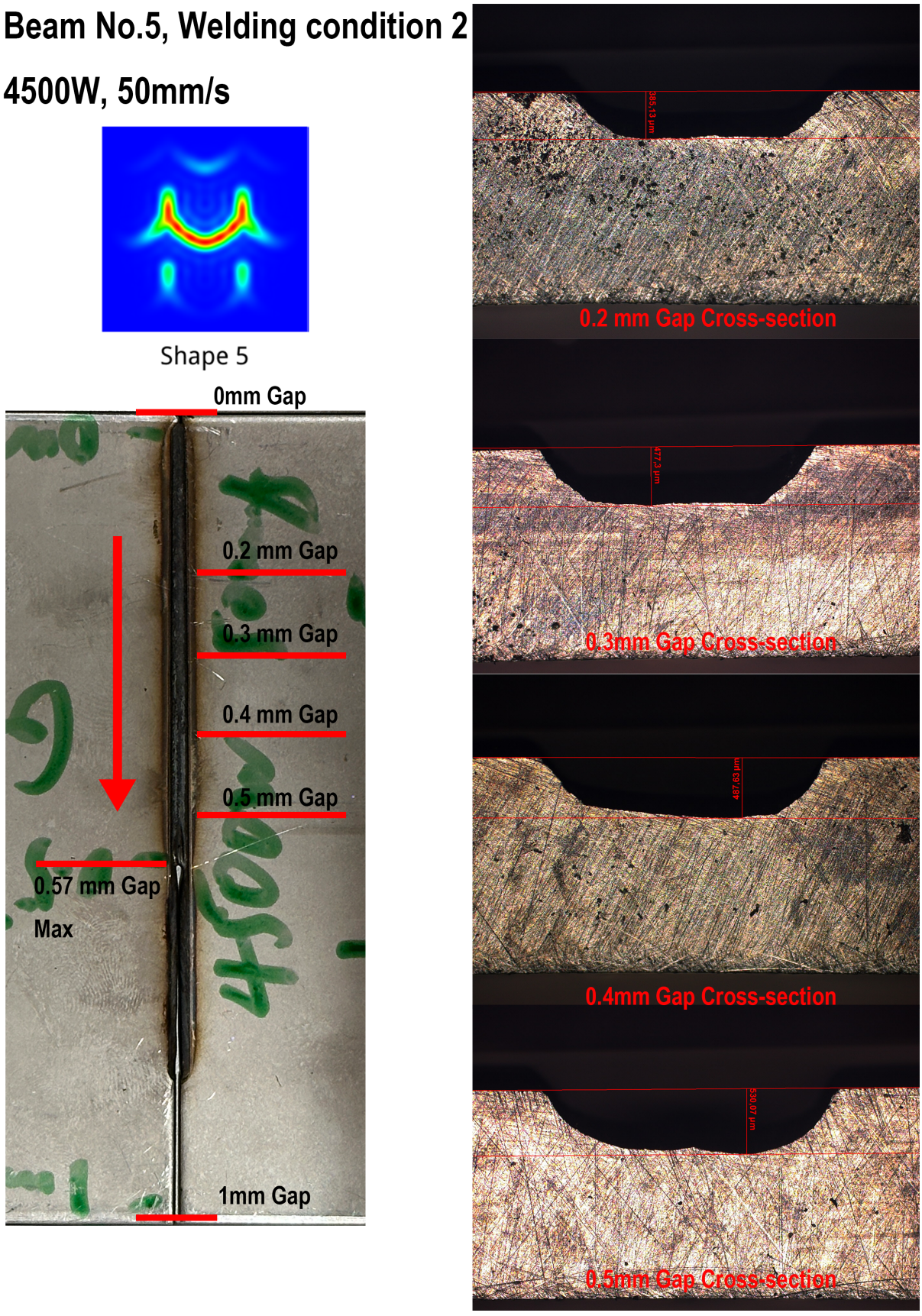

Figure A.5

Original Picture of shape 5 in welding condition 2

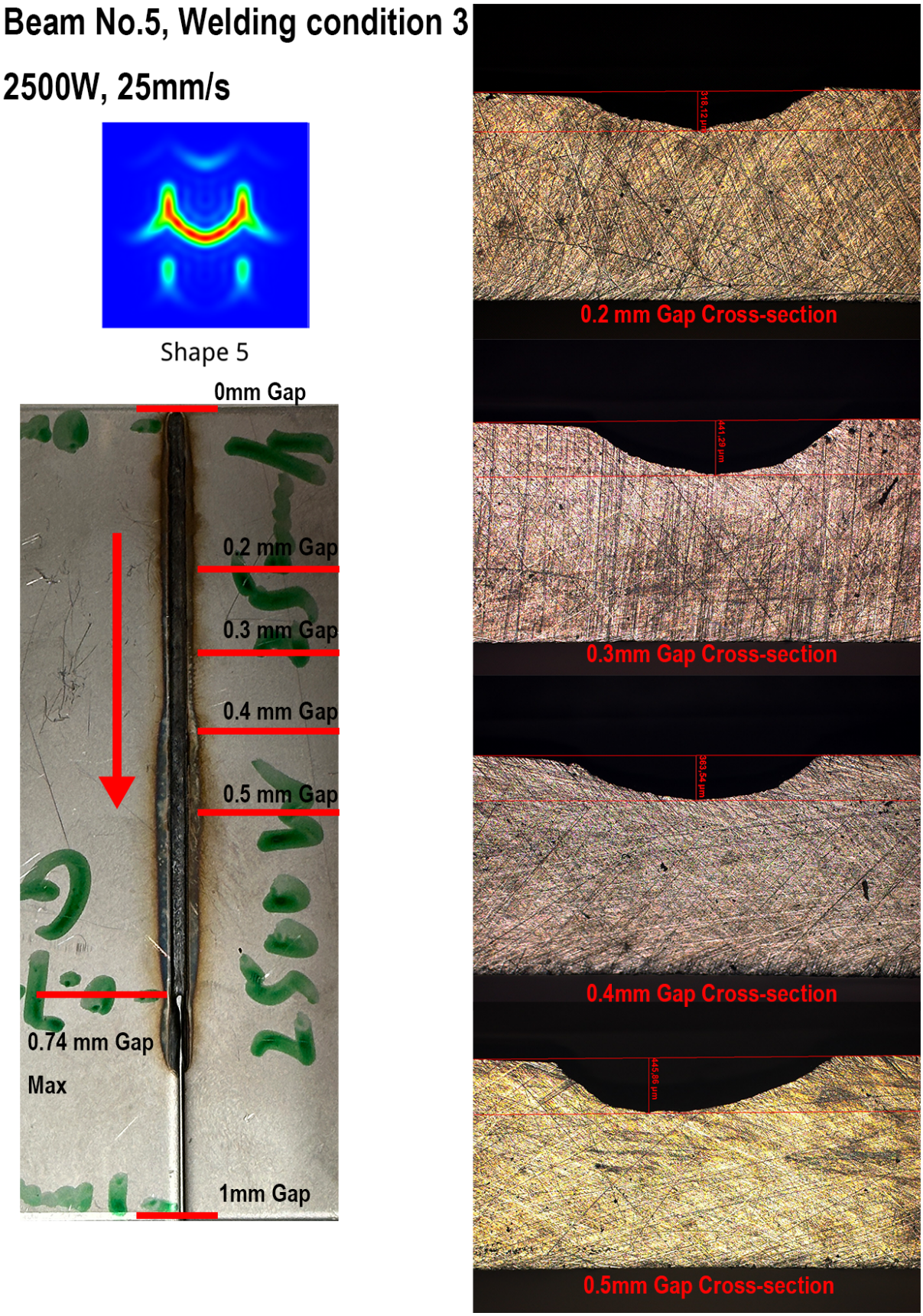

Figure A.6

Original Picture of shape 5 in welding condition 3

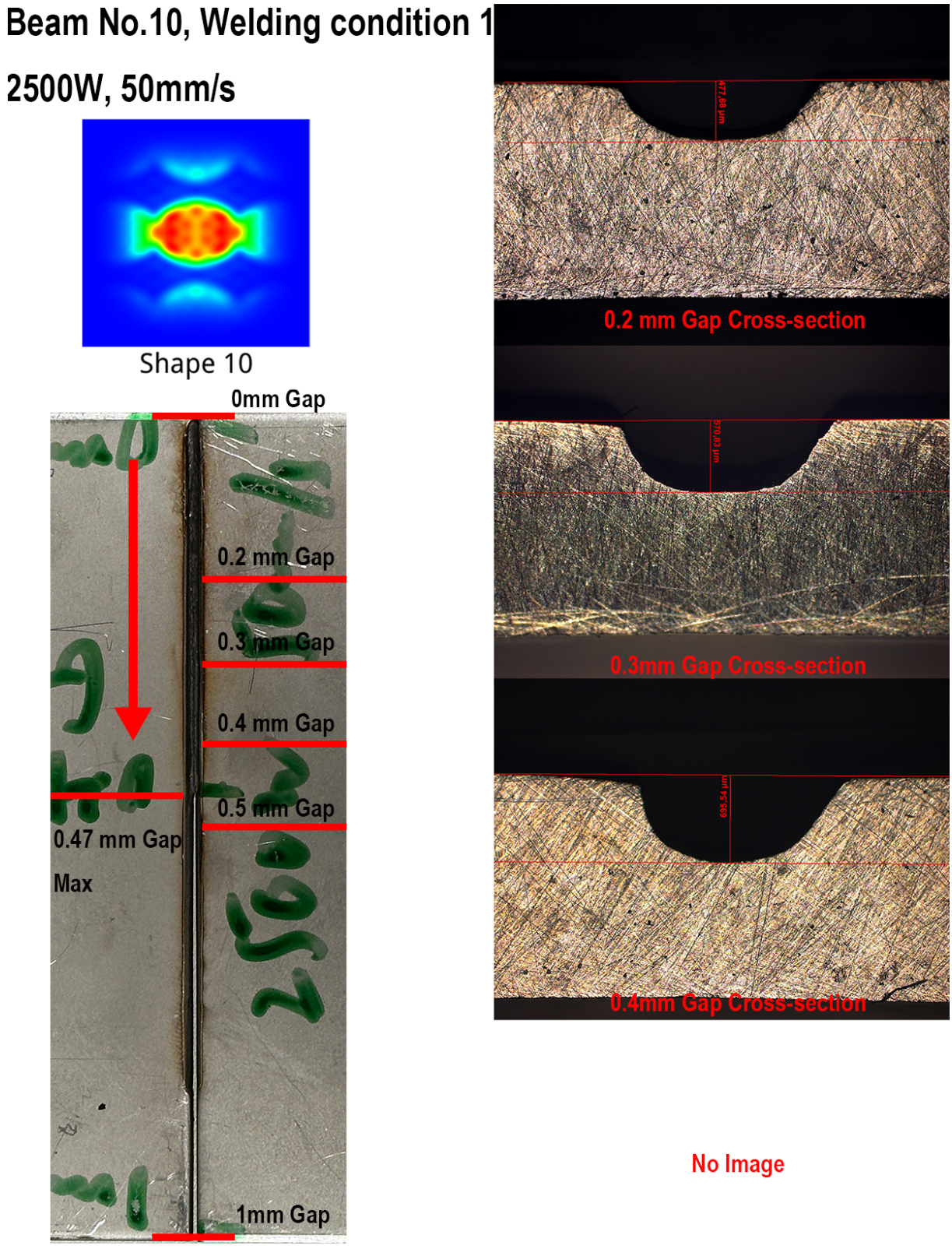

Figure A.7
Original Picture of shape 10 in welding condition 1

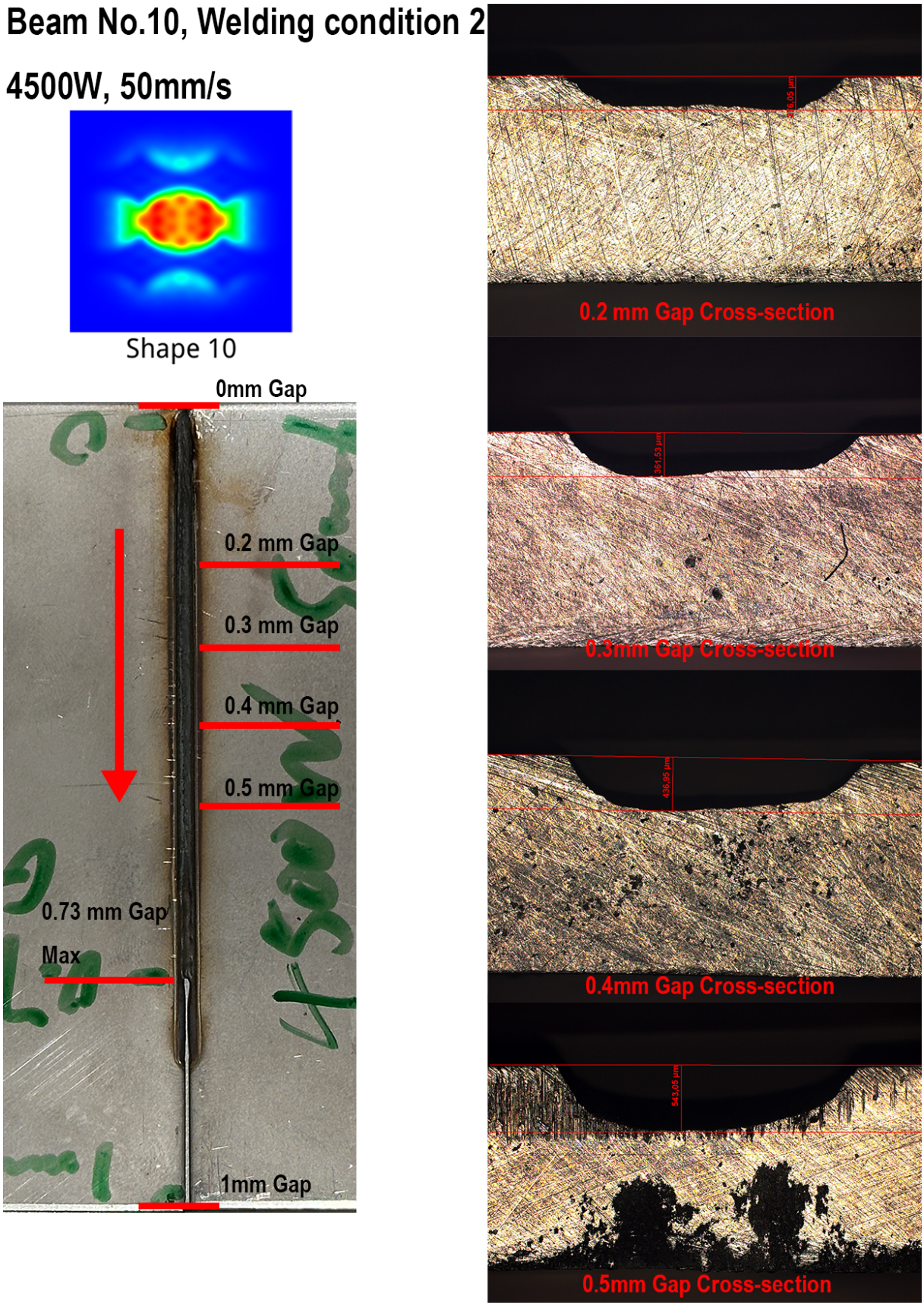

Figure A.8
Original Picture of shape 10 in welding condition 2

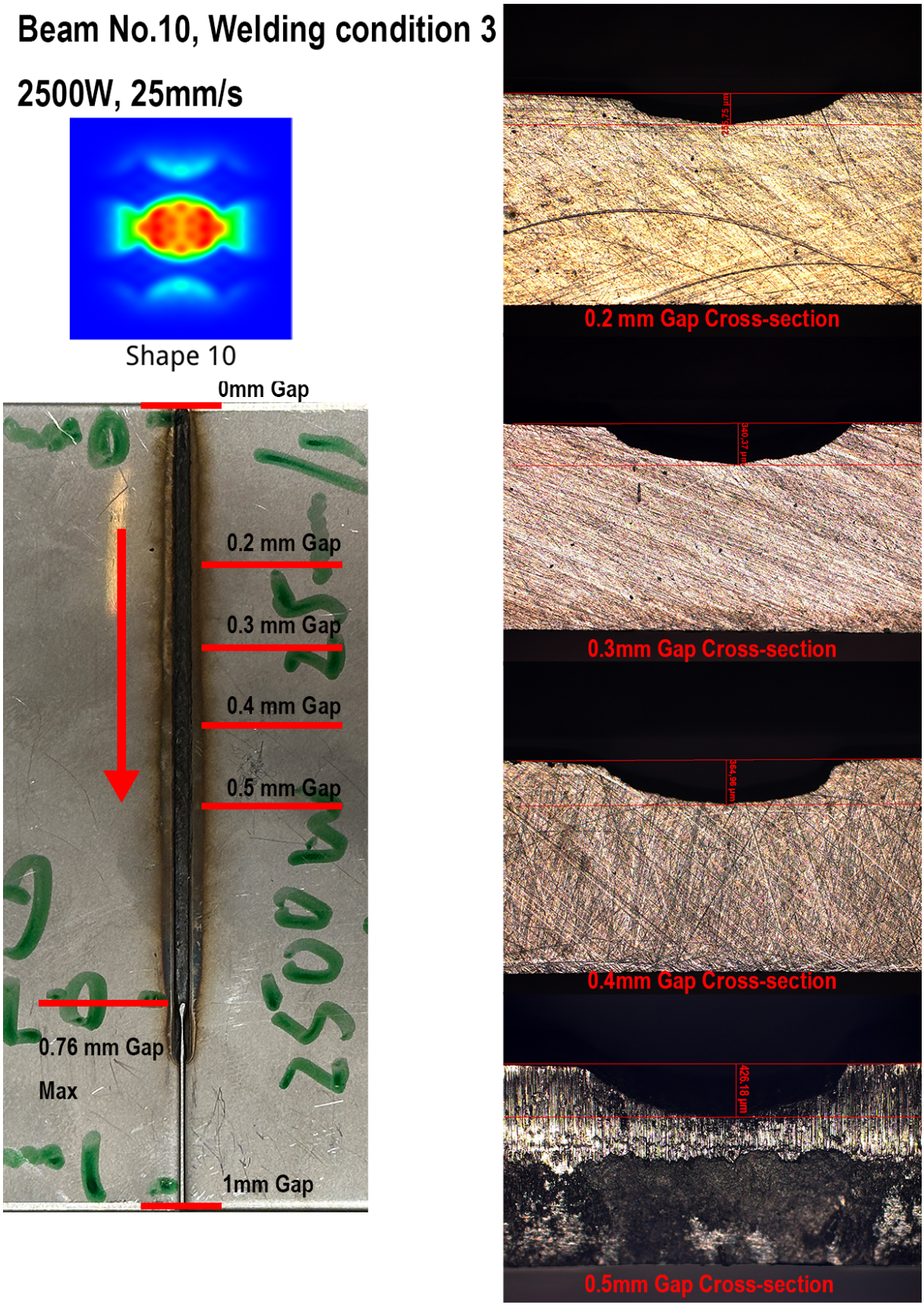

Figure A.9
Original Picture of shape 10 in welding condition 3